

Molecular dynamics study of ideal polymer chains with variable persistence length

Bachelor-Arbeit
zur Erlangung des Hochschulgrades
Bachelor of Science
im Bachelor-Studiengang Physik

vorgelegt von

Yahor Paromau
geboren am 29.12.1998 in Hrodna

Leibniz-Institut für Polymerforschung Dresden e. V.
Fakultät Physik
Bereich Mathematik und Naturwissenschaften
Technische Universität Dresden
2023

Eingereicht am 14. November 2023

1. Gutachter: Prof. Dr. Jens-Uwe Sommer
2. Gutachter: Prof. Dr. Arash Nikoubashman

Summary

Abstract

Utilizing molecular dynamics simulations, it is explored whether changes in the mechanical properties of the polymer chain, such as stiffness and friction coefficient of a terminal bead, may contribute to the observed by Singh *et. al* [10] alterations in scaling behavior. Additionally, while the dynamics of free chains have been studied extensively [9] [10], the dynamics of anchored semiflexible chains, as observed in the process of membrane tethering, remain relatively unexplored. This work aims to investigate the dynamical properties of anchored semiflexible chains while varying their stiffness and terminal bead radius. This study is conducted within the framework of ideal chain models, excluding hydrodynamic interactions. Results of this study reveal insights into the influence of chain stiffness and friction coefficient of the chain end on the dynamical properties of the chain in solution.

Kurzzusammenfassung

Mithilfe von Molekulardynamiksimulationen wird in dieser Arbeit untersucht, ob Veränderungen der mechanischen Eigenschaften einer Kette, wie Steifigkeit und Reibungskonstante des Endmonomers, zu den beobachteten Veränderungen im Skalierungsverhalten beitragen, wie sie von Singh *et al.* [10] festgestellt wurden. Während umfangreiche Forschung zur Dynamik freier Ketten durchgeführt wurde, ist die Dynamik von verankerten semiflexiblen Ketten, wie sie beim Prozess des Membrantetherings beobachtet werden, vergleichsweise wenig forscht. Diese Arbeit zielt darauf ab, die dynamischen Eigenschaften von verankerten semiflexiblen Ketten zu untersuchen, während ihre Steifigkeit und Reibungskonstante des Endmonomers der Endperle variiert werden. Die Arbeit erfolgt im Rahmen von Modellen idealer Ketten und schließt hydrodynamische Wechselwirkungen aus. Die Ergebnisse geben Einblicke in den Einfluss der Kettensteifigkeit und des Reibungskoeffizienten des Kettenendes auf ihre dynamischen Eigenschaften.

Contents

1. Introduction	7
1.1. Motivation and goal	7
1.2. Ideal polymer chain models	7
1.3. Langevin equation	9
1.4. Rouse model	9
1.4.1. Flexible chain	10
1.4.2. Semiflexible chain	13
2. Methods	15
2.1. Simulation methods	15
2.1.1. Molecular dynamics	15
2.1.2. Simulation setup	17
2.2. Evaluation methods	18
2.2.1. Measurement uncertainty	18
2.2.2. Main-axis coordinate system	18
2.2.3. Estimation of scaling exponent of MSD of ETE	18
2.2.4. Estimation of scaling behavior of MSDLM	19
3. Results	19
3.1. Anchored chain dynamics	20
3.1.1. Comparison to free chain	20
3.1.2. Impact of chain stiffness	22
3.1.3. Impact of the friction coefficient of the chain end	29
3.2. Free chain dynamics	35
4. Summary and Outlook	45
Appendices	48
A. Code	48
5. References	49

1. Introduction

1.1. Motivation and goal

Intracellular traffic represents an exciting realm, where the mechanisms of chemistry and mechanics are in harmony. An important process in this realm is pairing of small GTPases with long dimeric coiled-coil tether molecules [10], which is a part of a recent discussions in the literature [10]. Specifically, the process of membrane tethering was observed, driven by the conformational changes of the early endosomal tether EEA1, caused by its binding to the small GTPase Rab5 [8]. The conformational changes of EEA1 upon the binding of Rab5 are then closely studied by Singh *et al.* [10]. Among others they observed a change in the scaling behavior of the mean squared displacement of chains end upon the binding of the Rab5. They also have shown indirectly that this change is caused by a stiffness transition of the chain. However, the underlying molecules constitute a complex biological system, and there might be other factors affecting the change in the scaling behavior. With the help of coarse grained molecular dynamics simulations it is possible to investigate, if such change in the dynamical properties of the chain could be caused by the change of mechanical properties of the chain, such as stiffness and friction coefficient of the chain end, which is increased upon the binding of Rab5. Also, while the dynamical properties of free chains were already considered in various studies [10] [9] [6] [5], the dynamics of anchored semiflexible chains (as they occur in the process of membrane tethering, anchored to the endosome) is not yet well studied.

The goal of this work is, on the one hand, to study the dynamical properties of the anchored semiflexible chains by varying stiffness and friction of the chain end, on the other hand, to explore, if the above mentioned mechanical properties of the free chain can cause the change in scaling behavior of the chain, as observed by Singh *et al.* [10]. The scope of this work is limited by considering only ideal chain models and excluding hydrodynamic interactions.

1.2. Ideal polymer chain models

In the realm of polymer physics, ideal chain models serve as crucial tools for understanding the fundamental properties and behavior of polymer chains. These models provide simplified yet insightful descriptions of polymer chains' static properties and are integral to elucidating phenomena such as polymer persistence length and overall chain behavior. Ideal models are characterized by distinct assumptions concerning the permissible ranges of torsion and bond angles. Nevertheless, all these models disregard interactions between monomers that are widely spaced along the chain. In this section, 3 relevant ideal chain models are described: the freely jointed chain model, freely rotating chain model and the worm-like chain model.

Freely jointed chain model The freely jointed chain model is one of the simplest chain models. It assumes a constant bond length l_b [7] and no correlations between the directions of different bond vectors [7]: $\langle \cos(\theta_{ij}) \rangle = 0$ for $i \neq j$. This model is suitable to study properties of fully flexible polymer chains. Of particular interest are the end-to-end distance of the chain with N bonds

$$\langle R^2 \rangle = N l_b^2 \quad (1)$$

and the contour length

$$L = N l_b \quad (2)$$

Freely rotating chain model To define the polymer stiffness one needs to consider the polymer chain model where correlation between bond vectors does not vanish. The freely rotating chain (FRC) model is a fundamental ideal chain model that offers a simple yet valuable perspective on polymer behavior. This model assumes a constant bond length l_b [7], bond angles are constant [7] and all torsion angles are equally likely and independent of each other [7]. In this model there exists a correlation between bond vectors [7]:

$$\langle \vec{r}_i \vec{r}_j \rangle = l_b^2 (\cos(\theta))^{|j-i|} \quad (3)$$

A persistence segment of the chain is defined by the number of main-chain bonds s_p it contains [7]. This represents a scale at which local correlations between bond vectors decay [7].

$$s_p = -\frac{1}{\ln(\cos(\theta))} \quad (4)$$

The persistence length l_p of the chain is then defined as [7]:

$$l_p = l_b s_p \quad (5)$$

And the Kuhn length l_K of the chain is defined as [7]:

$$l_K = 2l_p \quad (6)$$

Worm-like chain model The worm-like chain model is a special case of the freely rotating chain model for small values of bond angles: $\theta \ll 1$ [7]. It is suitable for the description of very stiff polymers [7]. In this model the number of main-chain bonds in persistence segment simplifies to

$$s_p \approx \frac{2}{\theta^2} \quad (7)$$

The end-to-end distance of the chain can be evaluated as:

$$\langle R^2 \rangle = 2l_p L - 2l_p^2 \left(1 - \exp \left(-\frac{L}{l_p} \right) \right), \quad (8)$$

and the following relation holds between persistence length and angles of the chain:

$$\langle \cos(\theta_{ij}) \rangle = \exp \left(-\frac{l_b |j - i|}{l_p} \right), \quad (9)$$

which is useful if one needs to estimate the persistence length from the chain angles.

1.3. Langevin equation

The Langevin equation plays an important role in the description of the dynamics of polymer chains in a theta solvent [2]. The Langevin equation is a fundamental stochastic differential equation widely used in statistical mechanics and molecular dynamics to describe the dynamics of particles or molecules subjected to random forces in a dissipative medium. Specifically, the Langevin equation is used to describe the particle in immobile solvent and can be written as:

$$m\ddot{\vec{r}} = -\nabla U(\vec{r}) - \sigma m\dot{\vec{r}} + \vec{f}^r(t) \quad (10)$$

where: σ - damping constant, which accounts for the viscosity of the solvent, $\vec{f}^r(t)$ - stochastic force, which represents the effect of thermal fluctuations due to the particle's interactions with the solvent molecules and $U(\vec{r})$ - any external potential acting on the particle. $\vec{f}^r(t)$ is a stochastic process known as white noise, it is sampled from Gaussian distribution with zero mean $\langle \vec{f}^r(t) \rangle = 0$ and $\langle \vec{f}_\alpha^r(t) \vec{f}_\beta^r(t') \rangle = \lambda \delta(t - t')$, which relates strength of noise and friction. $\lambda = 2k_B T \sigma m$ and is known as fluctuation-dissipation theorem.

The solution of this equation depends of course on the selected external potential $U(\vec{r})$. In case of harmonic spring potential $U(\vec{r}) = \frac{1}{2}kr^2$ the formal solution can be written as [2]:

$$\vec{r}(t) = \frac{1}{\zeta} \int_{-\infty}^t dt' \exp \left(-\frac{t - t'}{\tau} \right) \vec{f}^r(t') \quad (11)$$

with $\zeta = m\sigma$ and $\tau := \zeta/k$. This equation is used further for the solution of the Rouse model for flexible chains and helps to derive [2] the equations for relevant observables.

1.4. Rouse model

Polymer chains, composed of repeating monomer units, exhibit complex behaviors that are of great interest in polymer physics and materials science. Understanding the dynamics of polymer chains is crucial for elucidating their mechanical, thermal, and transport properties.

One of the fundamental models used to describe polymer dynamics is the Rouse model.

The Rouse model is a widely used theoretical framework to study the dynamics of polymer chains in a theta solvent. This model simplifies the complex behavior of polymer chains by representing them as linear chains of noninteracting connected beads inside an immobile solvent.

1.4.1. Flexible chain

Firstly Rouse model for flexible free chains is introduced.

Assumptions The Rouse model makes certain key assumptions to facilitate its analytical treatment:

1. No hydrodynamic interactions or excluded volume effects between monomers.
2. Thermal forces acting on each bead follow Gaussian statistics.
3. Overdamped motion of the bead, which implies that inertia term vanishes: $m\ddot{\vec{r}} \approx 0$. Which is usually fulfilled in polymeric systems [1].
4. Beads continuously distributed along polymer chain [2].

Equation Assumptions 1, 2 lead to description of the system using the Langevin equation (Eq. 10). Following assumption 3 the inertia term is set to 0. The continuous approximation is then made as consequence of assumption 4. The initial equation of motion of single bead then becomes a diffusion equation [7]:

$$\zeta \frac{\partial \vec{r}(t, n)}{\partial t} = \frac{3k_B T}{l_b^2} \frac{\partial \vec{r}(t, n)}{\partial n^2} + \vec{f}^r(t) \quad (12)$$

with friction coefficient $\zeta = \sigma m$.

Boundary conditions The chain ends are connected to one spring only. Free ends could be modelled by introducing free boundary conditions. Two fictitious beads are added to both ends with $\vec{r}_0 = \vec{r}_1$ and $\vec{r}_N = \vec{r}_{N+1}$ [2]. The Boundary conditions for the diffusion equation can then be written as follows [2]:

$$\begin{aligned} \left(\frac{\partial \vec{r}}{\partial n} \right)_{n=0} &= 0 \\ \left(\frac{\partial \vec{r}}{\partial n} \right)_{n=N} &= 0 \end{aligned} \quad (13)$$

Solution The motion of the polymer can be decoupled in the motion of the independent modes using normal coordinates [2]. Define:

$$\vec{X}_p := \frac{1}{N} \int_0^N dn \cos\left(\frac{p\pi n}{N}\right) \vec{r}(n, t) \quad (14)$$

Eq. 12 can be then rewritten as [2]:

$$\zeta_p \frac{\partial}{\partial t} \vec{X}_p = -k_p \vec{X}_p + \vec{f}^p \quad (15)$$

with

$$\zeta_0 = N\zeta \text{ and } \zeta_p = 2N\zeta \text{ for } p = 1, 2, \dots \quad (16)$$

$$k_p = \frac{6\pi^2 k_B T}{Nl^2} p^2 \text{ for } p = 0, 1, 2, \dots \quad (17)$$

and \vec{f}^p is a random force, which satisfies [2]:

$$\begin{aligned} \langle f_{p\alpha} \rangle &= 0 \\ \langle f_{p\alpha}(t) f_{p\beta}(t') \rangle &= 2\delta_{pq}\delta_{\alpha\beta}\zeta_p k_B T \delta(t - t') \end{aligned} \quad (18)$$

This is a Langevin equation for the harmonic spring potential, with the formal solution [2]:

$$\vec{X}_p(t) = \frac{1}{\zeta_p} \int_{-\infty}^t dt' \frac{\exp(t - t')}{\tau_p} \vec{f}^p \quad (19)$$

with

$$\tau_p = \zeta_p / k_p \quad (20)$$

\vec{X}_p represents the local motion of the chain which includes $\frac{N}{p}$ segments and corresponds to the motion with the length-scale of the order $\sqrt{Nl_b^2/p}$ [2].

The inverse transformation of Eq. 14 is given by [2]:

$$\vec{r}_n = \vec{X}_0 + 2 \sum_{p=1}^{\infty} \vec{X}_p \cos(p\pi n/N) \quad (21)$$

Relevant observables In this paragraph the relevant dynamical quantities of rouse model are summarized. The important time scale is Rouse relaxation time τ_R :

$$\tau_R := \tau_1 = \frac{1}{3\pi^2} \frac{N^2 l_b^2 \zeta}{k_B T}, \quad (22)$$

which matches (except of factor $1/3\pi^2$) the time needed for the chain to diffuse over it's End-to-End distance. Other important time scale is relaxation time of the single monomer τ_0 :

$$\tau_0 = \frac{3\pi^2 \tau_R}{N^2} = \frac{l_b^2 \zeta}{k_B T}, \quad (23)$$

which matches the time needed for a free particle of size l_b to diffuse over a distance of it's own size, as described by the Langevin equation for the free particle. Time correlation of End-to-End (ETE) vector can be evaluated as [2]:

$$\langle \vec{R}(t) \vec{R}(0) \rangle = N l_b^2 \sum_{p=1,3,\dots} \frac{8}{p^2 \pi^2} \exp\left(\frac{-tp^2}{\tau_R}\right) \quad (24)$$

with the following asymptotic behavior [9]:

$$\langle \vec{R}(t) \vec{R}(0) \rangle = N l_b^2 \begin{cases} \frac{8}{\pi^2} \exp\left(\frac{-t}{\tau_R}\right) & \text{if } t \gg \tau_R \\ 1 - \sqrt{8t/(\pi^3 \tau_R)} & \text{if } t \ll \tau_R \end{cases} \quad (25)$$

Mean square displacement (MSD) of ETE is calculated as follows:

$$\begin{aligned} \langle [\Delta \vec{R}(t)]^2 \rangle &:= \langle [\vec{R}(t) - \vec{R}(0)]^2 \rangle \\ &= 2\langle R^2 \rangle - 2\langle \vec{R}(t) \vec{R}(0) \rangle \\ &= 2N l_b^2 \left(1 - \frac{8}{\pi^2} \sum_{p=1,3,\dots} \frac{1}{p^2} \exp\left(\frac{-tp^2}{\tau_R}\right) \right) \end{aligned} \quad (26)$$

with the asymptotic behavior:

$$\langle [\Delta \vec{R}(t)]^2 \rangle = 2N l_b^2 \begin{cases} (1 - \exp\left(\frac{-t}{\tau_R}\right)) & \text{if } t \gg \tau_R \\ \sqrt{8t/(\pi^3 \tau_R)} & \text{if } t \ll \tau_R \end{cases} \quad (27)$$

Also, one can see that the scaling behavior of $\langle [\Delta \vec{R}(t)]^2 \rangle$ is given by the scaling behavior of $\langle \vec{R}(t) \vec{R}(0) \rangle$ and the corresponding scaling exponent is $\alpha = \frac{1}{2}$. Further, MSD of chain end

(MSDLM) is evaluated as [11]:

$$\langle [\Delta \vec{r}_N(t)]^2 \rangle = \frac{2}{\pi^2} \langle R^2 \rangle \left(\sum_{p=1}^{\infty} \frac{1}{p^2} \left[1 - \exp \left(\frac{-tp^2}{\tau_R} \right) \right] + \frac{t}{\tau_R} \right) \quad (28)$$

with the following asymptotic behavior [11]:

$$\langle [\Delta \vec{r}_N(t)]^2 \rangle = N l_b^2 \begin{cases} \left(\frac{1}{3} + \frac{2t}{\pi^2 \tau_R} \right) & \text{if } t \gg \tau_R \\ \frac{2}{\pi^{3/2}} \sqrt{\frac{t}{\tau_R}} & \text{if } t \ll \tau_R \end{cases} \quad (29)$$

Extension to the anchored chains To describe the anchored chains, the boundary conditions must be adjusted to account for anchoring. Using the continuous approximation as described in [2], new boundary conditions can be evaluated as:

$$\begin{aligned} \left(\frac{\partial \vec{r}}{\partial n} \right)_{n=0} &= -\vec{r}_0 \\ \left(\frac{\partial \vec{r}}{\partial n} \right)_{n=N} &= 0 \end{aligned} \quad (30)$$

where \vec{r}_0 is the position of the fictitious bead as in the case of the free boundary conditions. Further, the possible solution path is sketched, however the solution itself remains outside of the scope of this work. In analogy with the case of the free chain, one needs to decouple the polymer motion in the modes of independent motion \vec{X}_p , which might in this case have a different expression than in the case of the free chain. Then, the diffusion equation is rewritten using obtained \vec{X}_p . The solution \vec{X}_p and the inverse transformation $\vec{r}_n(\{\vec{X}_p\})$ can eventually then be used to calculate relevant observables.

1.4.2. Semiflexible chain

The Rouse model prediction for semiflexible chains is more complicated as one need take into account the bending potential. The topic has already been studied, so the behavior of the observables $\langle \vec{R}(t)\vec{R}(0) \rangle$ and $\langle [\Delta \vec{r}_N(t)]^2 \rangle$ is available in the literature [9] for the asymptotic cases: rod limit $l_p \gg L$ and coil limit $l_p \ll L$.

Rod limit The behavior of the ETE autocorrelation function $\langle \vec{R}(t)\vec{R}(0) \rangle$ in the rod limit ($l_p \gg L$) is given by [9]:

$$\langle \vec{R}(t)\vec{R}(0) \rangle \propto \begin{cases} \exp(-t/\tau_{rot}) & \text{if } t > \tau_1; l_p \gg L \\ \exp[-\frac{8\Gamma(1/4)}{3\pi} \frac{L}{l_p} (\frac{t}{\tau_1})^{3/4}] & \text{if } \tau_0 < t < \tau_1; l_p \gg L \end{cases} \quad (31)$$

with τ_1 given by [9]:

$$\tau_1 \approx \tau_0 L^4 / (l_p l_b^3) \quad \text{if } l_p \gg L \quad (32)$$

and τ_{rot} given by [9]:

$$\tau_{rot} \approx \tau_0 (L/l_b)^3 \quad (33)$$

and Γ referring to Γ -function. The case $\tau_0 < t < \tau_1$ for $\tau_0 < t \ll \tau_1$ can be approximated as [9]:

$$\langle \vec{R}(t) \vec{R}(0) \rangle \propto 1 - \frac{8\Gamma(1/4)}{3\pi} \frac{L}{l_p} \left(\frac{t}{\tau_1} \right)^{3/4} \quad \text{if } \tau_0 < t \ll \tau_1; l_p \gg L \quad (34)$$

which delivers a $\alpha = \frac{3}{4}$ scaling exponent of the ETE autocorrelation function of a free chain in the rod limit.

The behavior of MSDLM $\langle [\Delta \vec{r}_N(t)]^2 \rangle$ in rod limit ($l_p \gg L$) on short time scales is given by [9]:

$$\langle [\Delta \vec{r}_N(t)]^2 \rangle \approx l_b^2 \left(\frac{l_b}{l_p} \right)^{1/4} \left(\frac{t}{\tau_0} \right)^{3/4} \quad \text{if } \tau_0 < t < \tau_1; l_p \gg L \quad (35)$$

One observes the same scaling exponent as in case of MSD of ETE: $\alpha = \frac{3}{4}$. However, on the time scale, on which free diffusion takes place, the scaling exponent remains unchanged relative to the flexible chain and is given by $\alpha = 1$, because chain stiffness does not affect the chain translational diffusion as a whole [9].

Coil limit In the coil limit $l_p \ll L$ there are several timescales [9]:

$$\begin{aligned} \tau_1 &\approx \tau_0 \left(\frac{l_p}{l_b} \right)^3 \quad \text{if } l_p \ll L \\ \tau_{rot} &\approx \frac{L^2 l_p \tau_0}{l_b^3} \quad \text{if } l_p \ll L \\ \tau_R &\propto \tau_{rot} \quad \text{if } l_p \ll L, \end{aligned} \quad (36)$$

τ_1 is not equals τ_1 (Eq. 20) from predicton of Rouse model for fully flexible chains. On the timescale $t \ll \tau_1$ the autocorrelation function of the ETE is given by [9]:

$$1 - \langle \vec{R}(t) \vec{R}(0) \rangle \propto \frac{l_p}{L} \left(\frac{t}{\tau_1} \right)^{3/4} \quad \text{if } t \ll \tau_1, l_p \ll L \quad (37)$$

On the timescale $\tau_1 < t \ll \tau_R$ the equations are given by the Rouse model predictions for flexible chains renormalized in space $l_b \rightarrow l_p$ and in time $\tau_0 \rightarrow \tau_1$ [9]. The scaling exponent is then given by $\alpha = 1/2$ [9]. The crossover from $\alpha = 1/2$ to $\alpha = 3/4$ is expected for $t = \tau_1$ [9].

On the timescale $t > \tau_{rot}$ the following regime holds [9]:

$$\langle \vec{R}(t) \vec{R}(0) \rangle \propto \exp(-t/\tau_{rot}) \quad \text{if } t > \tau_{rot}, l_p \ll L \quad (38)$$

2. Methods

2.1. Simulation methods

2.1.1. Molecular dynamics

Molecular dynamics (MD) is a powerful computational technique that provides insight into the dynamic behavior of molecular systems by time-integrating the Newton's equations of motion for each atom or particle. In the context of polymer physics, MD simulations offer a detailed view of how polymer chains evolve over time, enabling the exploration of their conformational changes, interactions, and mechanical properties.

For the purpose of this study, the Large-scale Atomic/Molecular Massively Parallel Simulator (LAMMPS) [13] is employed, a widely used software package for molecular dynamics simulations. LAMMPS facilitates the simulation setup and integration algorithms necessary to investigate the behavior of polymer chains with varying persistence length and boundary conditions.

Integrator In this study, the velocity-Verlet algorithm is employed as the numerical integrator. This algorithm updates particle positions and velocities over discrete time steps, providing an accurate and stable trajectory for the simulation. It involves the following steps [12]:

1. Calculate position: $\vec{r}(t + \Delta t) = \vec{r}(t) + \vec{v}(t)\Delta t + \frac{1}{2}\vec{a}(t)\Delta t^2$
2. Derive $\vec{a}(t + \Delta t)$ from the interaction potential using $\vec{r}(t + \Delta t)$
3. Calculate $\vec{v}(t + \Delta t) = \vec{v} + \frac{1}{2}(\vec{a}(t) + \vec{a}(t + \Delta t))\Delta t$

Bond potential The finite extensible nonlinear elastic (FENE) potential [6] is used to model the bonds between neighbouring-monomers. This is a standard choice for bead-spring polymer models [13]. The potential equation used in LAMMPS can be written as [13]:

$$U_{bond}(r) = \begin{cases} -\frac{1}{2}kR_0^2 \ln \left[1 - \left(\frac{r}{R_0} \right)^2 \right] + 4\epsilon \left[\left(\frac{\sigma_{LJ}}{r} \right)^{12} - \left(\frac{\sigma_{LJ}}{r} \right)^6 \right] + \epsilon & \text{if } r \leq 2^{1/6}\sigma_{LJ} \\ -\frac{1}{2}kR_0^2 \ln \left[1 - \left(\frac{r}{R_0} \right)^2 \right] & \text{if } 2^{1/6}\sigma_{LJ} < r \leq R_0 \\ 0 & \text{else} \end{cases} \quad (39)$$

with R_0 - the maximum extent of the bond, k - spring constant, ϵ - parameter regulating the depth of the potential minimum, σ_{LJ} - parameter regulating the location of the minimum of the potential. The potential consists of an attractive (first) and a repulsive (Lennard-Jones, second) term which is set to 0 if r is larger than the minimum ($2^{1/6}\sigma_{LJ}$) of the Lennard-Jones potential.

Bending potential An entropic worm-like potential [11] is introduced to control the persistence length of the chain [11]. The potential is defined by:

$$U_{bend}(\theta) = \kappa(1 - \cos(\theta)) \quad (40)$$

Thermostat A Langevin thermostat is used to regulate the temperature of the system and interaction with the solvent. The Langevin thermostat emulates the interactions between particles and a heat bath, introducing stochastic forces to individual particles that mimics the effects of thermal fluctuations, as well as interactions between particles and solvent by a friction force acting on individual particles. The equations of motion for individual particles then take the form of a Langevin equation as described in section 1.3, aside from some implementation-driven properties of the random force \vec{f}^r :

1. $\vec{f}^r \propto \sqrt{k_B T m \sigma \frac{1}{dt}}$ where dt is the integration timestep [13]
2. A random number sampled from a uniform distribution is used to randomize the direction and magnitude of this force instead of Gaussian random number to speedup the calculations [13] [3].

Boundaries Periodic boundary conditions (PBC) are introduced to mimic the behavior of an infinite system. This approach eliminates boundary effects and creates a virtual environment where particles interact as if they were part of a continuous and unbounded space. Under PBC, when a particle exits one edge of the simulation box, it re-enters from the opposite edge, maintaining the illusion of a seamless and infinite system. This study includes only the interaction between bonded monomers and adjacent bonds, so the problem of "image" interactions, which would occur with long-range interactions, is excluded.

2.1.2. Simulation setup

Chosen simulation settings and parameters are explained in this section.

A LJ unit system is used, in which mass, $\sigma_{LJ}, \epsilon, k_B = 1$ and the masses, distances, energies are specified as multiples of these values [13].

The simulation box has a side length 200 and periodic boundary conditions in all dimensions are used. The polymer chain is modelled as series of interconnected beads, where each bead represents a monomer, and the bonds represent the bonds between monomers. The adjacent connected beads of the chain interact according to FENE potential $U_{bond}(r)$, as introduced in section 2.1.1, with parameters: $K = 30.0$, $R_0 = 1.5$, $\epsilon = 1.0$, $\sigma_{LJ} = 1.0$. The angles between adjacent bonds of the same chain are affected by the bending potential $U_{bend}(\theta)$, as described in section 2.1.1 and κ is varied to obtain the desired Kuhn length according to equation [11]:

$$l_K = l_b \begin{cases} \frac{2\kappa + \exp(-2\kappa) - 1}{1 - \exp(-2\kappa)(2\kappa + 1)} & \text{if } \kappa > 0 \\ 1 & \text{if } \kappa = 0 \end{cases} \quad (41)$$

The simulation box is populated with 500 chains. Each chain consists of 64 monomers of mass $m = 1$ and initial bond length $l_b = 0.97$ with its first monomer at the origin and is created using random walk. The chains do not interact between each other and hence form an ensemble of 500 chains. In case of simulations with larger chain ends the mass of the end monomer is set $m_e = 1.5$. In case of experiments with large values of Kuhn length the angles are randomized in the way to have more straight chain to resulting in decreasing number of steps to achieve the equilibrium.

The temperature of the system and forces on the beads are controlled with Langevin thermostat with parameters: $\text{damp} = \frac{1}{\sigma} = 1.0$, $T = 1.0$. In following, the friction coefficient of the bead $\zeta = m\sigma = 1$, unless said otherwise. In case of anchored chain the forces acting on first two beads of the chain are set to 0 pinning the chain to the origin and excluding rotational degrees of freedom.

The mean bond length is $l_b = 0.97$. The variation of the bond length over considered κ (Eq. 39) range is assumed to be negligibly small [11], and therefore l_b is assumed to be constant.

The simulation initially runs until it reaches the equilibrium and then the measurements of particle trajectories are performed.

2.2. Evaluation methods

2.2.1. Measurement uncertainty

In this work the 99.73% confidence interval is used, which means $\approx 99.7\%$ of observations would land in the given confidence interval. Gaussian error propagation is used to propagate the uncertainty. The normal distribution is assumed everywhere, where the measurement uncertainty is given.

2.2.2. Main-axis coordinate system

To analyze the dynamics of the anchored chain, the main-axis coordinate system is introduced. In this system the z axis is parallel to the first bond vector, connecting the first two beads, which are fixed. The orthonormal basis set, that defines the system, is calculated as follows:

$$\hat{z}_{MA} = \frac{\vec{r}_1 - \vec{r}_0}{\|\vec{r}_1 - \vec{r}_0\|} \quad (42)$$

$$\hat{y}_{MA} = \begin{cases} (\hat{x} + \hat{y}) \times \hat{z}_{MA} & \text{if } \hat{x} \parallel \hat{z}_{MA} \\ \hat{x} \times \hat{z}_{MA} & \text{otherwise} \end{cases} \quad (43)$$

$$\hat{x}_{MA} = \hat{z}_{MA} \times \hat{y}_{MA} \quad (44)$$

where \hat{x} , \hat{y} , \hat{z} are the vectors of the standard basis.

2.2.3. Estimation of scaling exponent of MSD of ETE

The MSDLM in the case of free chains obeys the relationship [10]:

$$\langle [\Delta \vec{r}_N(t)]^2 \rangle \propto t^{\alpha(t)} \quad (45)$$

with $\alpha(t)$ being the scaling exponent. Therefore, $\alpha(t)$ of MSDLM can be calculated using following equation [10]:

$$\alpha(t) = \frac{\partial \log(\langle [\Delta \vec{r}_N(t)]^2 \rangle)}{\partial \log(t)} \quad (46)$$

We then make an assumption, that the MSD-ETE of anchored chains obeys the same proportionality as the MSDLM of free chains (Eq. 45). Therefore, $\alpha(t)$ of the MSD-ETE can be

calculated using the following relationship:

$$\alpha(t) = \frac{\partial \log(\langle [\Delta \vec{R}(t)]^2 \rangle)}{\partial \log(t)} \quad (47)$$

To estimate $\alpha(t)$ of the MSD-ETE curve the following algorithm is applied:

1. Split the MSD by the time (t/LJ) in n bins logarithmically using `numpy.logspace` [4]
2. Within each bin:
 - a) Calculate: $x = \log_{10}(t)$, $y = \log_{10}(\text{MSD})$
 - b) Shift to origin: $x = x - \min(x)$, $y = y - \min(y)$
 - c) Use `scipy.optimize.curve_fit` [14] to fit the $f(x) = \alpha x$ to the x, y , obtaining α , the scaling exponent within the bin.

Measurement uncertainty of the scaling exponent, $\Delta\alpha$, is estimated by calculating the measurement uncertainty of y , Δy , from the measurement uncertainty of the MSD-ETE (MSD), ΔMSD :

$$\Delta y = 3\sigma_y = 3 \frac{1}{\text{MSD} \ln(10)} \sigma_{\text{MSD}} \quad (48)$$

where σ_y is the standard deviation of y and σ_{MSD} is the standard deviation of MSD. σ_y is then supplied to the `scipy.optimize.curve_fit` [14], when calculating α . The algorithm outputs the variance-covariance matrix, from which σ_α , and, therefore, $\Delta\alpha = 3\sigma_\alpha$ can be calculated.

2.2.4. Estimation of scaling behavior of MSDLM

To estimate the scaling behavior $\alpha(t)$ of the MSDLM curve (Eq. 45, Eq. 46), a similar algorithm as in case of MSD-ETE is applied, except that instead of splitting the curve into the bins, the rolling window of size defined in log scale is used. Basically $\alpha(t_i)$ is calculated using linear regression, as previously mentioned, on the rolling window defined by $|\log_{10}(t) - \log_{10}(t_i)| \leq w$ with w being the logarithmic window size. The step of the rolling window is 1 element. Per default $w = 1$ (which matches a decade-long window) unless an other value is mentioned.

3. Results

This section unveils the outcomes of an investigation into the dynamic characteristics of anchored and free polymer chains. The focus of the study lies in assessing the impact of two properties: chain stiffness and the friction of the (free) chain end.

3.1. Anchored chain dynamics

Firstly, this study focuses on a comparative analysis between the dynamics of anchored polymer chains and their free counterparts. To execute this comparison, the focus is narrowed onto a specific dynamical quantity - the mean squared displacement of the end-to-end distance (MSD of ETE) further referred to as MSD.

3.1.1. Comparison to free chain

In this section, the investigation focuses on understanding the influence of anchoring on chain dynamics. This is achieved by comparing the MSD of a fully-flexible anchored chain with the predictions provided by the Rouse model. According to the Rouse model predictions for the free full flexible chain, the MSDLM of such chain has 3 regions or scaling regimes: anomalous diffusion region, $\text{MSDLM} \propto t^{1/2}$, $\alpha = 1/2$, intermediate or crossover region, where the transition from anomalous diffusion to the free diffusion takes place and free diffusion region, $\text{MSDLM} \propto t$, $\alpha = 1$, because of the chain movement as a whole. However, for the anchored full flexible chain is expected, that in the crossover region of MSD or MSDLM the transition occurs from anomalous diffusion region, $\alpha = 1/2$, to the $\alpha = 0$ region, because the chain is anchored. By contrasting simulation results with theoretical expectations, insights are gained into how anchoring affects chain dynamics.

Figure 1 shows, that by anchoring the chain the transition into a plateau is shifted to the right, increasing the relaxation time (Eq. 22), however the scaling behavior is visually the same. The Rouse relaxation time of the free chain predicted using the Rouse model (with the same parameters as in the simulation, Section 2.1.2) is: $\tau_R = 130.16$ (Eq. 22), $\tau_0 = 0.941$ (Eq. 23). The Rouse relaxation time of the anchored chain estimated using the fit of the Eq. 26 with τ_R as free parameter to the MSD curve of acnhored chain is: $\tau_R = 555 \pm 62$, $\tau_0 = 4.1 \pm 0.5$, which is approximately 4 times larger. One needs to take into account, that the bond potential used in the simulations, FENE (Eq. 39), does not match the bond potential used in the Rouse model, harmonic spring potential. Therefore, it is also necessary to compare the above-mentioned results with the simulation of the free chain. On the Figure 1 is shown, that the predictions of the Rouse model match the results of the simulation of the free chains within the confidence interval. The Rouse relaxation time of the free chain, estimated using the fit of the Eq. 26 with τ_R as free parameter to the MSD curve of free chain is $\tau_R = 138.6 \pm 14.3$, $\tau_0 = 1.0 \pm 0.1$, which matches, within the confidence interval, the one analytically (using Eq. 22, Eq. 23) calculated. The usage of τ_R as free parameter to describe the MSD of anchored chains relies on the assumption, that the dynamics of anchored chain obeys the same equations as dynamics of free chain, but with different time scales. The fitted curve is displayed on Figure 2. The match of the fitted curve to the simulation data indirectly verifies this assumption. Intuitively such difference is clear, the beginning of the anchored chain can't move and therefore the chain needs more time to achieve the MSD limit, which in case of fully flexible free chain is $2Nl_b^2$ as

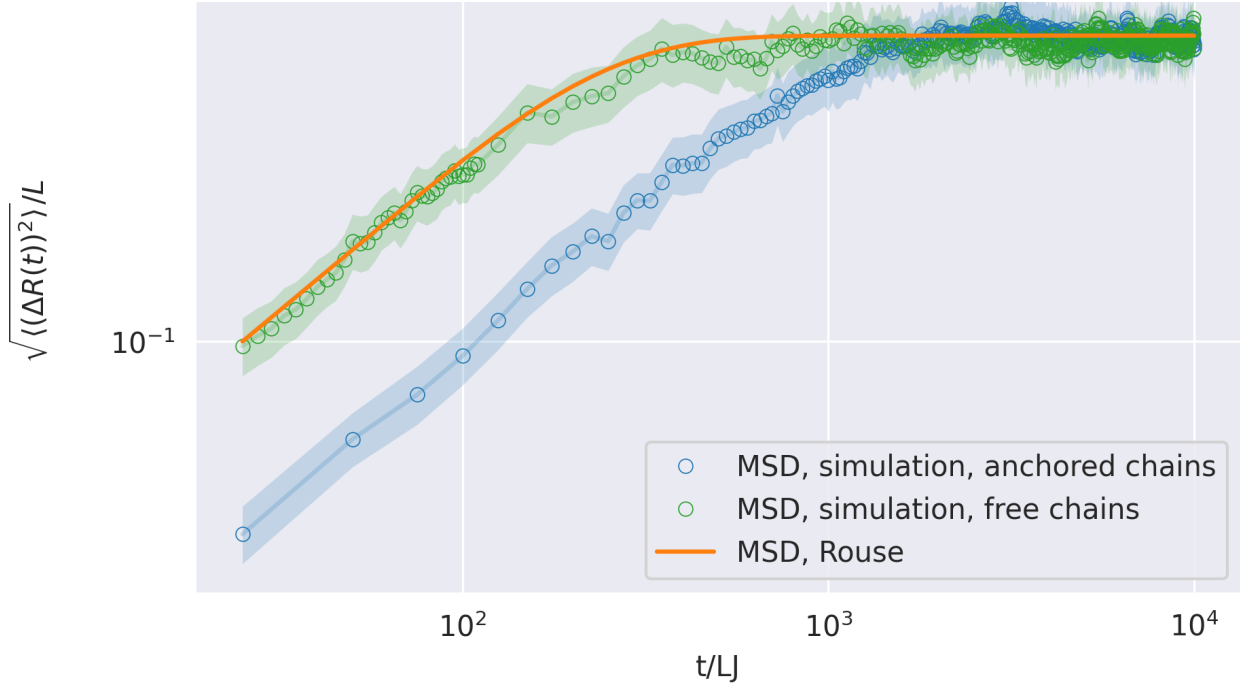


Figure 1: MSD of ETE of an anchored fully flexible chain and MSD of ETE of a free fully flexible chain vs predictions of the analytical Rouse model (free chain, Eq. 26). The filled area corresponds to the MSD curve ± 3 standard deviations of the mean. The line connecting data points and the filled area between data points doesn't make any statements about probability of measuring values in this interval and is added for readability.

the one can see from Eq. 26.

It is possible to introduce correction factor based on the estimated τ_R to account for the boundary conditions:

$$\beta := \frac{\tau_{0,\text{simulation,anchored}}}{\tau_{0,\text{analytical, free}}} \approx 4.26 \quad (49)$$

In this section predictions of the analytical Rouse model for the free fully flexible chains were compared to the data obtained from the simulation of the anchored fully flexible chains. It has been found, that analytical Rouse model predictions of the MSD of the free fully flexible chain (Eq. 26) can describe the anchored chain, if τ_R is considered as free parameter. However, we note, that the predictions for anchored fully flexible chains can probably be obtained analytically by solving the Rouse model within the anchored boundary conditions (Eq. 30) and the predictions obtained using the fit are not equivalent to the predictions derived analytically. The comparison of analytically calculated τ_R (Eq. 22) of the free chain with estimated τ_R of the anchored chain revealed, that τ_R of the anchored chain is significantly (4 times) larger. Finally, the correction factor β for τ_0 was introduced to account for anchoring.

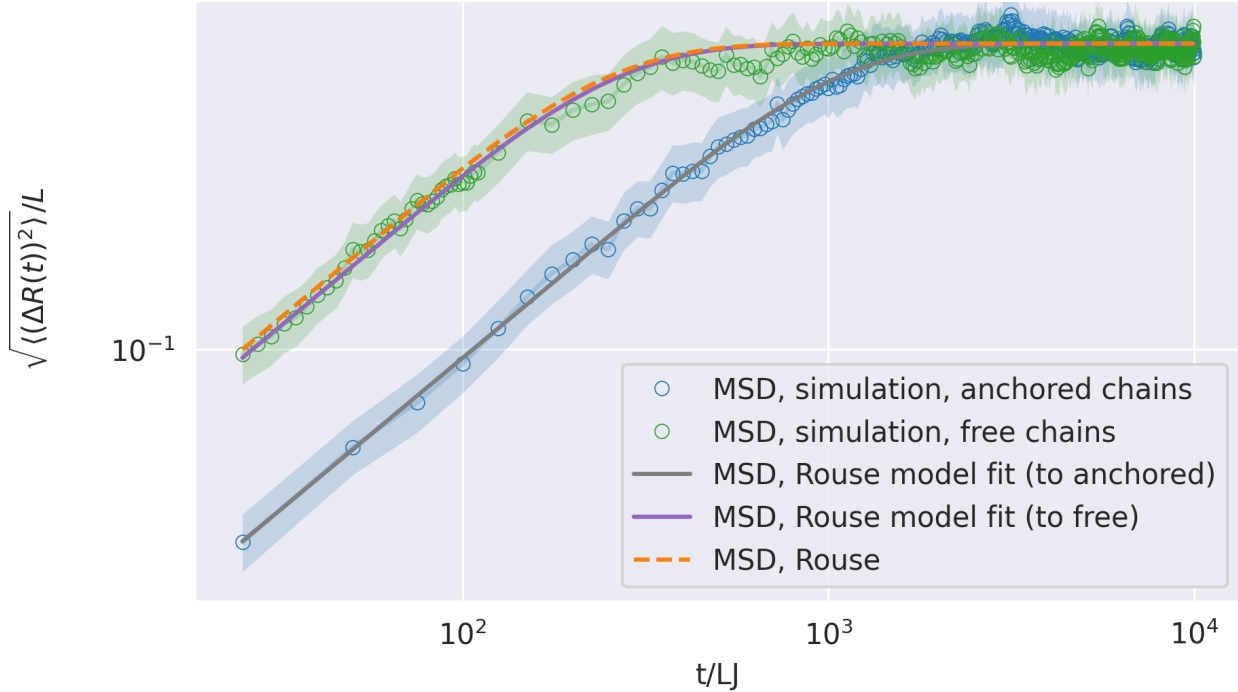


Figure 2: MSD of ETE of an anchored fully flexible chain (blue points) and MSD of ETE of a free fully flexible chain (green points). Fit of the modified rouse model prediction (Eq. 26) with τ_R as a free parameter to the MSD of ETE of an anchored fully flexible chain (grey line) and to the MSD of ETE of a free fully flexible chain (purple line). The filled area corresponds to the MSD curve ± 3 standard deviations of the mean. The blue line connecting data points and the filled area between data points doesn't make any statements about probability of measuring values in this interval and is added for readability.

3.1.2. Impact of chain stiffness

Within this subsection, the focus shifts toward exploring the influence of chain stiffness on the dynamics of anchored chains. By manipulating the angle potential (Eq. 40) the MSD curves for different values of the Kuhn length l_K were measured. The analysis provides insights into how varying the chain stiffness exert an influence on the dynamics exhibited by anchored chain. Table 1 shows the range of stiffness values examined in this set simulations.

The MSD curves are plotted in Figure 3 and the logarithmic representation is given in Figure 3b. The following observations are made:

- The relaxation time grows non-linearly with increasing l_K
- The long time MSD limit grows non-linearly with increasing l_K , however for $l_K/L >= 0.65$ it is not possible to distinguish the curves any more because of the uncertainty.

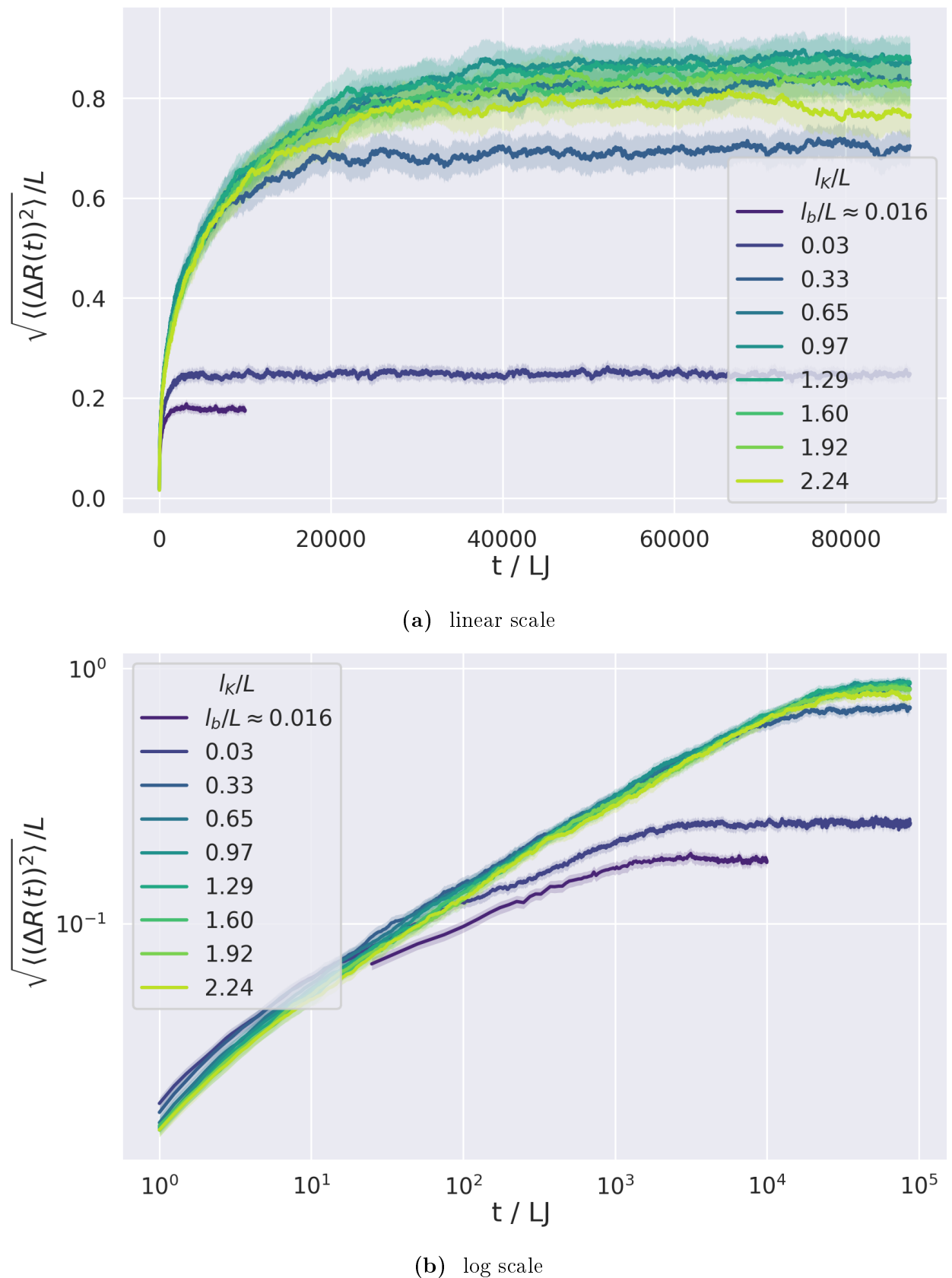


Figure 3: Empirical MSD of ETE of anchored chains with different Kuhn length values. Filled area corresponds MSD curve ± 3 standard deviations of the mean.

κ	N_K	l_K/L
0.00	63.00	$l_b/L \approx 0.016$
1.00	32.96	0.03
11.00	3.00	0.33
21.00	1.54	0.65
31.00	1.03	0.97
41.00	0.78	1.29
51.00	0.62	1.60
61.00	0.52	1.92
71.00	0.45	2.24

Table 1: Values of κ and corresponding l_K tried in the study of anchored chain dynamics. Contour length $L = 61.11$.

Comparison with the Rouse model predictions for flexible chains Further, the empirical results are compared to the predictions of the Rouse model. Firstly, the empirical results are compared to the Rouse model predictions for the fully flexible chain with N_K segments of length l_K . The results of this comparison are shown in Figure 4. Then the empirical results are compared to the Rouse model predictions for fully flexible chain with τ_R as free parameter. The results of this comparison are displayed in Figure 5. It is clear, that the Rouse model predictions for fully flexible chain doesn't match the observed behavior of semiflexible anchored chains even with τ_R as free parameter. This result matches the intuition, that deviations from the Rouse model predictions for the free, fully flexible chains increase with increasing l_K , because semiflexible chains require separate and more complicated description (section 1.4.2), than the fully flexible ones within the Rouse model.

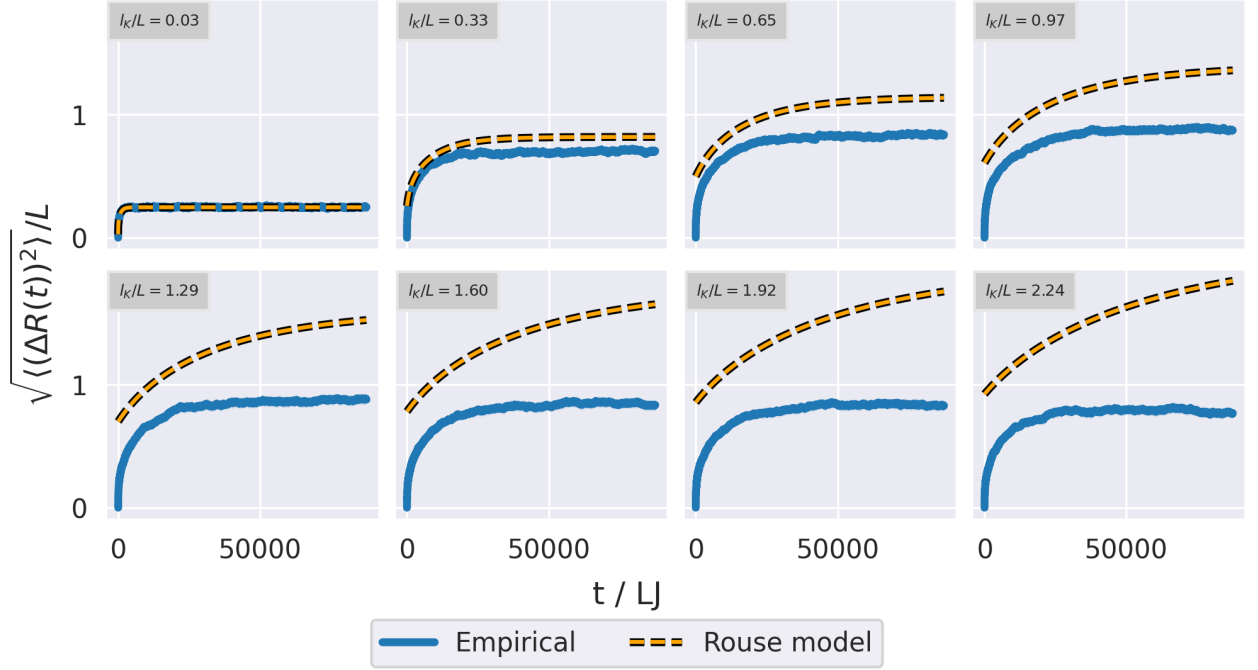


Figure 4: Empirical MSD of ETE of anchored chains with different Kuhn length values and Rouse model prediction for fully-flexible chains (Eq.26) with $N_b = N_K$ if $N_K \geq 1$ or $N_b = 1$ otherwise. τ_R adjusted using β (Eq.49) to account for boundary conditions.

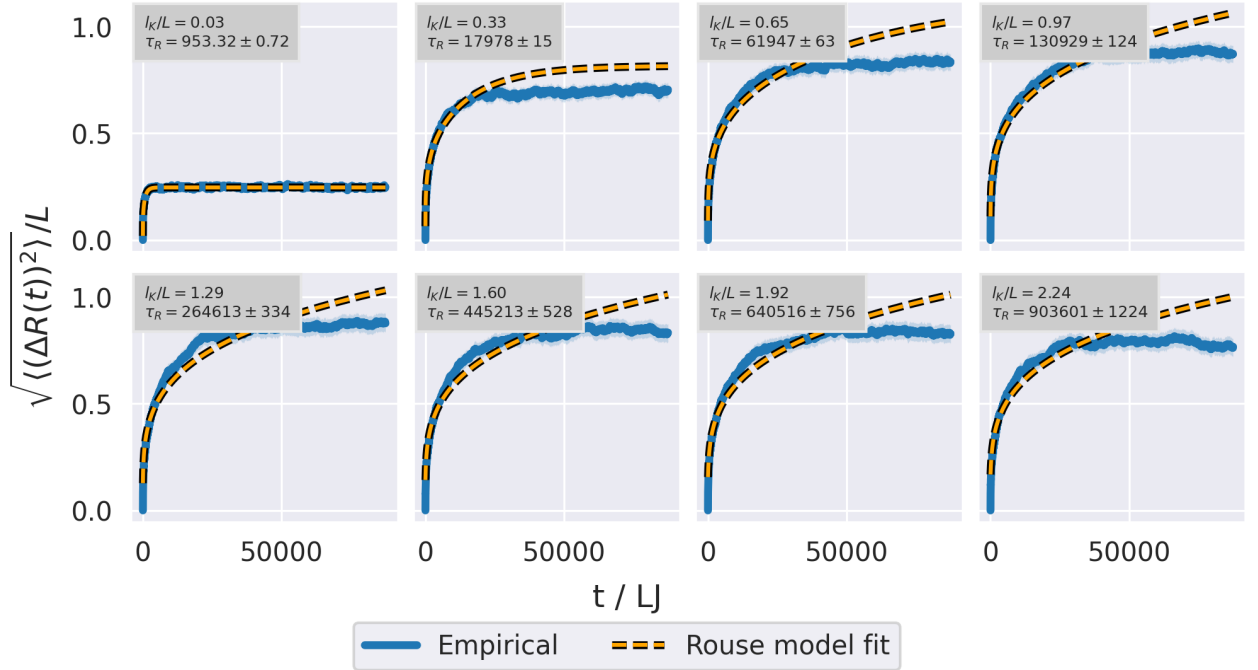


Figure 5: Empirical MSD of ETE of anchored chains with different Kuhn length values and fit of Rouse model prediction for fully-flexible chains (Eq.26) with $N_b = N_K$ if $N_K \geq 1$ or $N_b = 1$ otherwise. τ_R is free parameter. The summation in Eq.26 does not extend to N_K as it should strictly do, but up to the number of bonds (63) of the fully flexible chain.

Comparison with Rouse model predictions for semiflexible chains Furthermore, the empirical MSD curves are compared to the predictions of the Rouse model for the semiflexible chains. The autocorrelation function of the End-to-End vector was already discussed in Section 1.4.2. The MSD can be written as

$$\langle [\Delta \vec{R}(t)]^2 \rangle = \langle R^2(t) \rangle - 2\langle \vec{R}(t)\vec{R}(0) \rangle + \langle R^2(0) \rangle = 2(\langle R^2 \rangle - \langle \vec{R}(t)\vec{R}(0) \rangle)$$

where the term $\langle \vec{R}(t)\vec{R}(0) \rangle$ in case of free semiflexible chain obeys the relationships discussed in Section 1.4.2.

To compare the long time case with empirical results, the expression $2(\langle R^2 \rangle - k \exp(-t/\tau_{rot}))$ with k as free parameter was fitted to the part of the corresponding empirical MSD curves as specified in Eq. 38 and Eq. 31. The result was then visually examined against the empirical curve. This comparison revealed, that MSD in long time limit based on Eq. 38 and Eq. 31 does not correspond to the empirical curves. However, an introduction of two meaningful free parameters (a, τ_{rot}) is able to dismiss the discrepancy between theoretical approach for the free chain and empirical results for the anchored chain:

$$\langle [\Delta \vec{R}(t)]^2 \rangle = a \langle R^2 \rangle \left[1 - \exp\left(-\frac{t}{\tau_{rot}}\right) \right] \quad (50)$$

This equation is referred further as "Adjusted Rouse model". The free parameter a accounts the for large-time limit of MSD and τ_{rot} accounts for the location of the transition into the plateau. However, one can only speculate, whether the new τ_{rot} has the same meaning as the old one. The results of this fit are shown in Figure 6. It is possible to conclude, that in case of anchored chains the proportionality $\langle \vec{R}(t)\vec{R}(0) \rangle \propto \exp(-\frac{t}{\tau_{rot}})$ holds for $t > \tau_{rot}$ but with a different value (and eventually meaning) of τ_{rot} . In case of the chains close to the rod-limit one can see that in analogy with the case of free chains in the rod limit there should be some analogy of characteristic time τ_1 (from Eq. 31), which is smaller than the simulated τ_{rot} , and where the above mentioned proportionality starts to be valid.

Further, the case of short times is examined. To execute this comparison, the scaling behavior of the empirical MSD is analyzed. It is clear, that $\langle [\Delta \vec{R}(t)]^2 \rangle \propto t^{\alpha(t)}$ for the small times is valid in analogy to the scaling behavior of MSD of the last monomer of the free chain. The scaling exponent α is estimated from the MSD curves as described in Section 2.2.3 with $n = 10$ bins. The result is shown on Figure 7. Further in this paragraph α_{min} refers to the scaling exponent α in the region in which the overdamped motion takes place and $t \ll \tau_{rot}$. For the nearly flexible chain $l_K/L = 0.03$ $\alpha_{min} \approx \frac{1}{2}$ is observed, which matches theoretical expectations for fully flexible chain (section 1.4.1). For semiflexible chains the value α_{min} is close to $\frac{3}{4}$, which matches the scaling behavior of free chain at short times. One can see, that α_{min} gets closer to $\frac{3}{4}$ with rising l_K . Larger scaling factor in the region [1, 10] is due to transition from ballistic

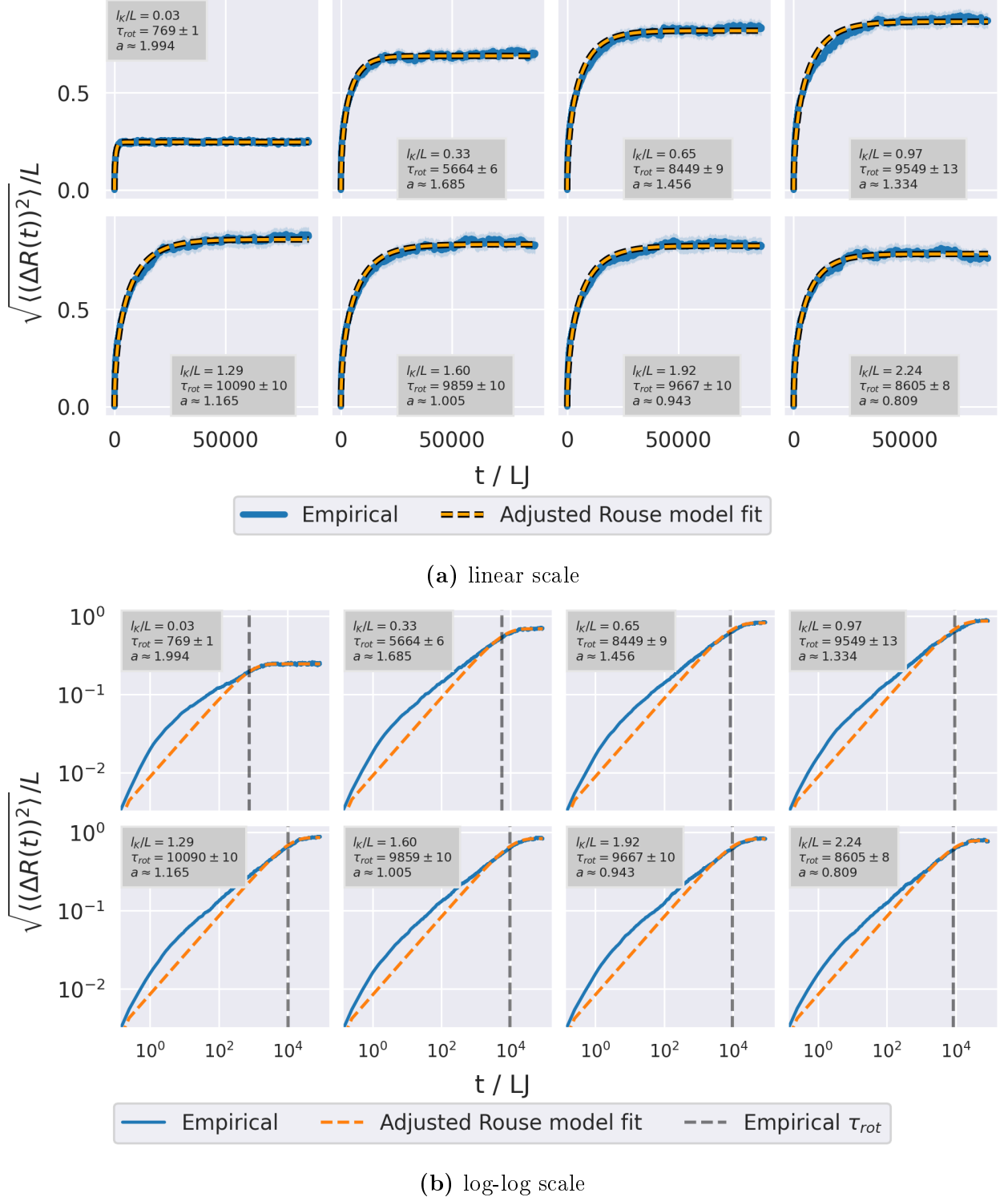


Figure 6: Empirical MSD of ETE of anchored chains with different Kuhn length values (blue line), and fit of the modified Rouse model prediction for semiflexible chains (Eq.50, dashed line) on log-log scale. Estimated (empirical) τ_{rot} is drawn as vertical dashed line.

motion at time scales $t < \frac{1}{\sigma} = 1$ to the overdamped motion. Additionally, α for $t > \tau_{rot}$ matches the one of rouse model prediction for free semiflexible chain as well as α transitions in this regime smoothly near the τ_{rot} .

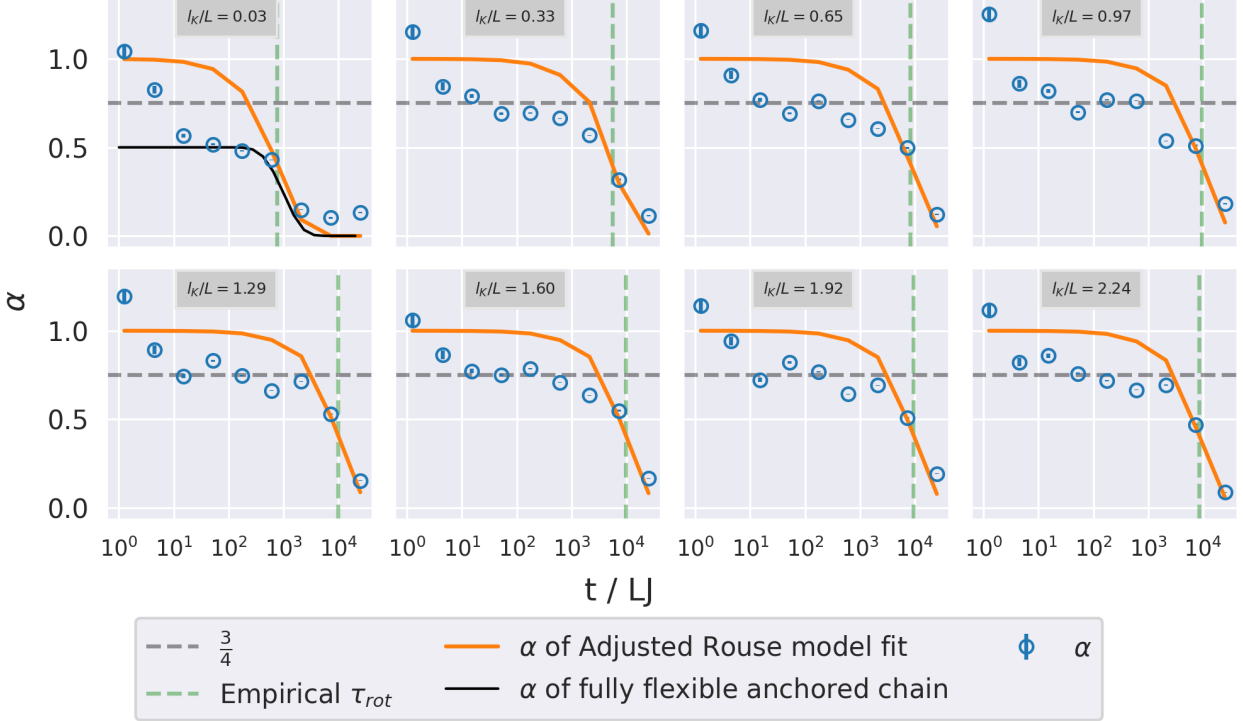


Figure 7: Scaling exponent α of the MSD of ETE of anchored semiflexible chain (blue points) and scaling exponent α of the Adjusted Rouse model prediction for semi-flexible chains (Eq.50, orange line). Estimated (empirical) τ_{rot} is drawn as vertical dashed line. Horizontal grey dashed line corresponds to $\frac{3}{4}$ value. Black line on the top left plot corresponds to the scaling exponent α of the modified Rouse model prediction (Eq. 26 with τ_R as free parameter, estimated in section 3.1.1, $\tau_R \approx 582.3$) for anchored flexible chains as explained in section 3.1.1.

Separation of the dynamics into components parallel and perpendicular to the main-axis Further, the MSD in main-axis coordinate system (section 2.2.2) is analyzed. Figure 8 shows the MSD curves in main axis system for each dimension. The analysis delivers following insights:

- The difference of MSD in z dimension relative to the x and y dimensions rises with growing stiffness. The plateau value of MSD falls.
- The MSD in z dimension has smaller relaxation time in case $l_K/L \geq 0.95$

The chain becomes more straight with rising stiffness and therefore has less freedom of movement along the z direction, which results in a smaller MSD and quicker relaxation.

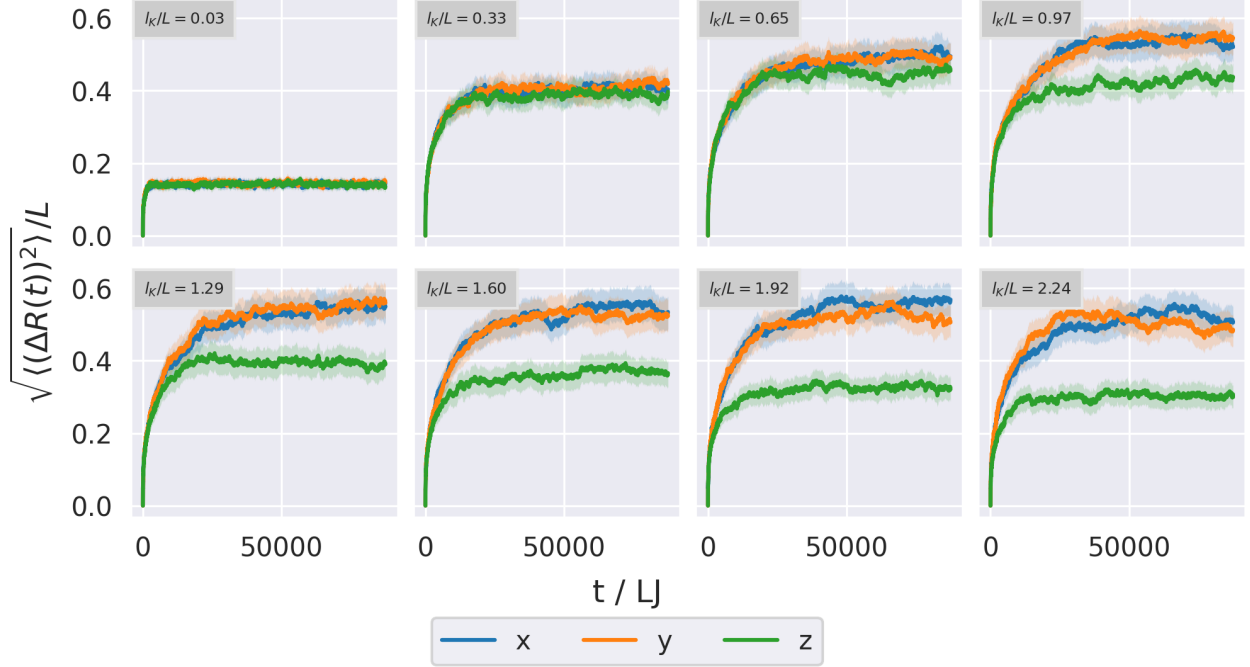


Figure 8: Empirical MSD of ETE of anchored chains with different Kuhn length values in main-axis coordinate system (See section 2.2.2). For reasons of the system's symmetry, the x and y components have to behave identically.

3.1.3. Impact of the friction coefficient of the chain end

In this subsection, the focus turns to the influence of the friction coefficient at the chain end on the dynamics of anchored chain with high stiffness.

In the simulation this is achieved by changing the value of the damping constant of the Langevin thermostat for the last bead of the chain. Assuming the Stokes friction, changing the value of the damping parameter effectively means a change of the bead diameter. The mass of the end bead is set to the $m_e = 1.5$ (a modification of the mass is arbitrary, but it affects the damping time $\tau_d = m_e/\zeta_e$) and friction coefficient of end bead is varied: $\zeta_e = 10, 15$, which corresponds to the end-bead diameters: 15, 30. The reference value provides simulation of the chain with $\zeta_e = \zeta = 1$ and $m_e = m = 1$. In all 3 cases $\kappa = 190.2$, which results in Kuhn length $l_K/L = 6.02$. The chosen persistence length of the chains relative to their contour length $l_p/L = l_K/(2L) = 3.01$ matches the one of the unbound EEA1 [10].

Comparison with the Rouse model The approach mostly follows section 3.1.2 with an exception that the friction coefficient of the chain end ζ_e is varied instead of Kuhn length l_K of the chain. The resulting MSD curves are shown on Figure 9. Again, the adjusted Rouse model (Eq. 50) is fitted to the MSD curves (Figure 10). One can see the perfect match on time scales $t > \tau_{rot}$. Also, the estimated τ_{rot} rise with rising ζ_e and the scaling behavior on short time scales

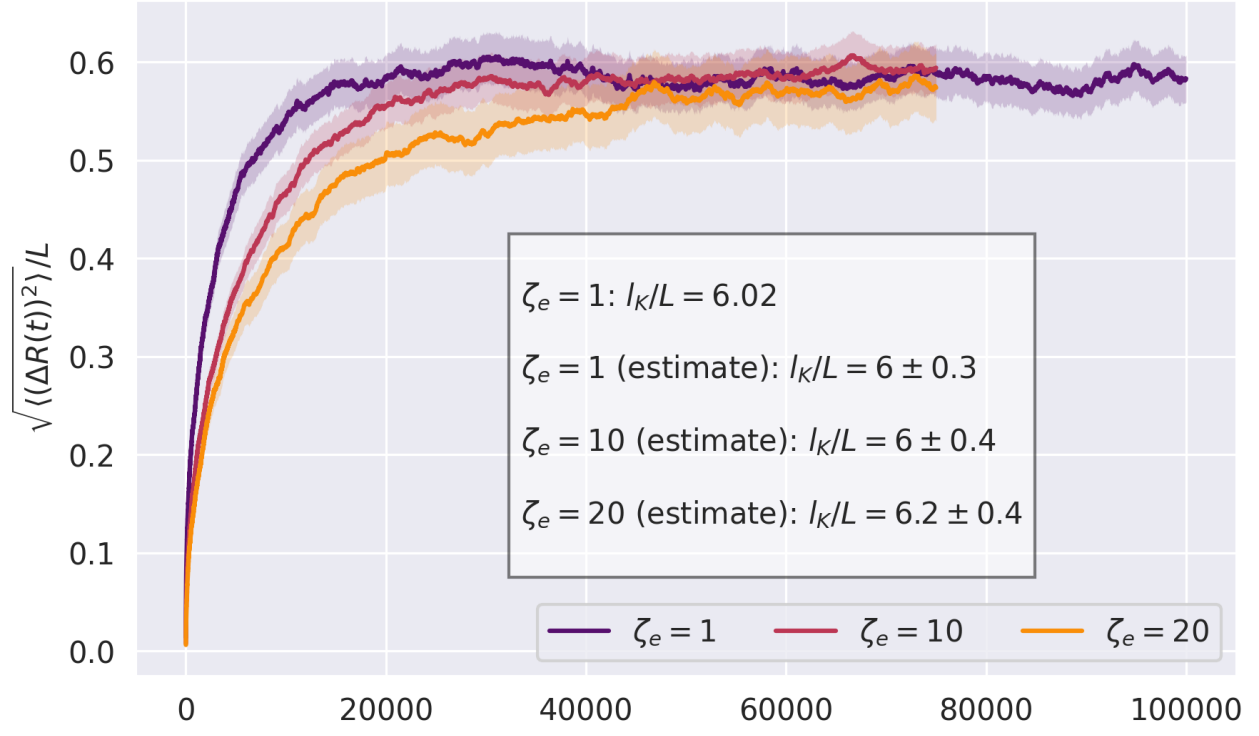
varies. To investigate the scaling behavior, the scaling exponent α is calculated as described in section 2.2.3 within $n = 20$ bins and is plotted on Figure 11. The Rouse model for semiflexible free chains predicts $\alpha = 3/4$ on the time scales $t < \tau_1 \ll \tau_{rot}$. To test if this holds for chains with larger friction coefficient of the chain end it's necessary to estimate α in this region. We define $\alpha_m := \alpha$ for $t \ll \tau_{rot}$. Based on *Nikoubashman et. al.* [9] finding, that the crossover from ballistic motion to anomalous diffusion, as described in Rouse model, lasts 2 decades of time, it is assumed, that the left boundary of this region is given by the end of the region of the crossover from the ballistic motion to the anomalous diffusion of the end bead, $\tau_b := 10 \frac{m}{\zeta_e}$. The right boundary is assumed to be $\tau_{rot}/10$ to match $t \ll \tau_{rot}$ requirement. The boundaries of the region are plotted as a red dashed line and vizually match the observed scaling behavior. α_m is then calculated as the mean of observed α in the region. The measurement uncertainty is estimated as 3 standard deviations of the mean. All estimated quantities are summarized in Table 2. One can see the small increase of α_m by transition from $\zeta_e = 1$ to $\zeta_e = 10$ and, given the confidence interval, there is no difference between α_m for $\zeta_e = 10$ and $\zeta_e = 20$.

Separation of the dynamics into components parallel and perpendicular to the main-axis Additionally different dimensions of the MSD in main-axis coordinate system are analyzed and the results are shown on Figure 12. One can observe, that the visual patterns of increasing ζ_e for all dimensions are the same.

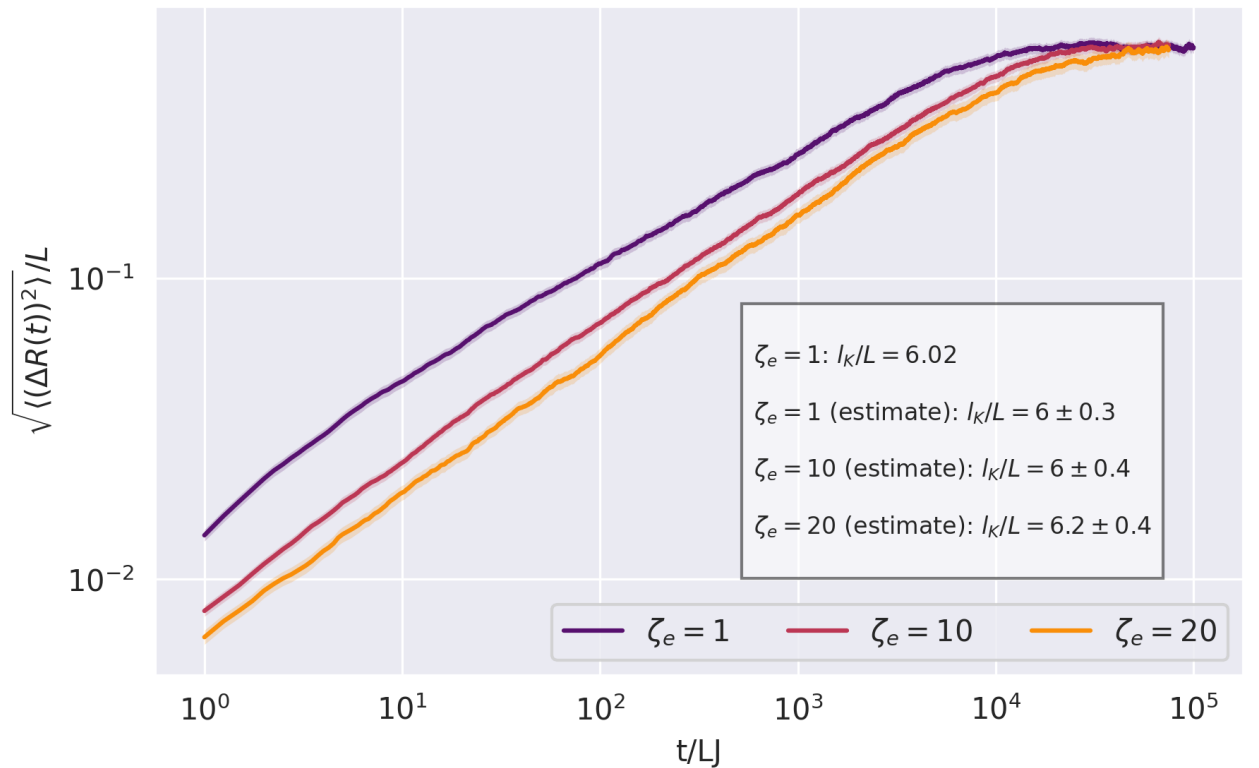
Summary To summarize the findings of Section 3.1.2, we note: A higher friction of the chain end slows down the overall dynamics of the chain and leads to a delayed plateau phase. The expected (Eq. 31) proportionality for longer time scales $\langle \vec{R}(t)\vec{R}(0) \rangle \propto \exp\left(-\frac{t}{\tau_{rot}}\right)$ holds for $t > \tau_{rot}$, however estimated τ_{rot} have different value and eventually meaning than the analytical one (Eq. 33). Also, Figure 10b shows, that there might be some analogy of characteristic time $\tau_1 < \tau_{rot}$ (Eq. 32) where above mentioned proportionality starts to be valid in analogy with Rouse model predictions for the free semiflexible chains. On shorter timescales $t \ll \tau_{rot}$ scaling exponent α increases (Table 2) when ζ_e is increased from 1.0 to 10.0 and is not in agreement with Rouse model predictions for free semiflexible chains (section 1.4.2). Long term limits of are not affected by the damping constant.

ζ_e	τ_{rot}	$\Delta\tau_{rot}$	a	Δa	m_e	α_m	$\Delta\alpha_m$
1	4914.250775	2.551632	0.381353	0.000096	1.0	0.736970	0.055872
10	9863.543716	3.602848	0.387068	0.000071	1.5	0.919990	0.067072
20	11967.770149	7.068073	0.357454	0.000103	1.5	0.928494	0.070997

Table 2: Anchored chain, $l_K/L = 6.02$. Estimated values of free parameters of Adjusted Rouse model (Eq.50), estimated scaling exponent α_m and corresponding ζ_e and m_e values.



(a) linear scale



(b) log-log scale

Figure 9: Empirical MSD of ETE of anchored chains with different values of the friction coefficient of the chain end ζ_e . Configured and estimated Kuhn length is shown in the text box (as additional check of plausibility). An estimate of the Kuhn length is done using a fit of Equation 9 with l_p as free parameter.

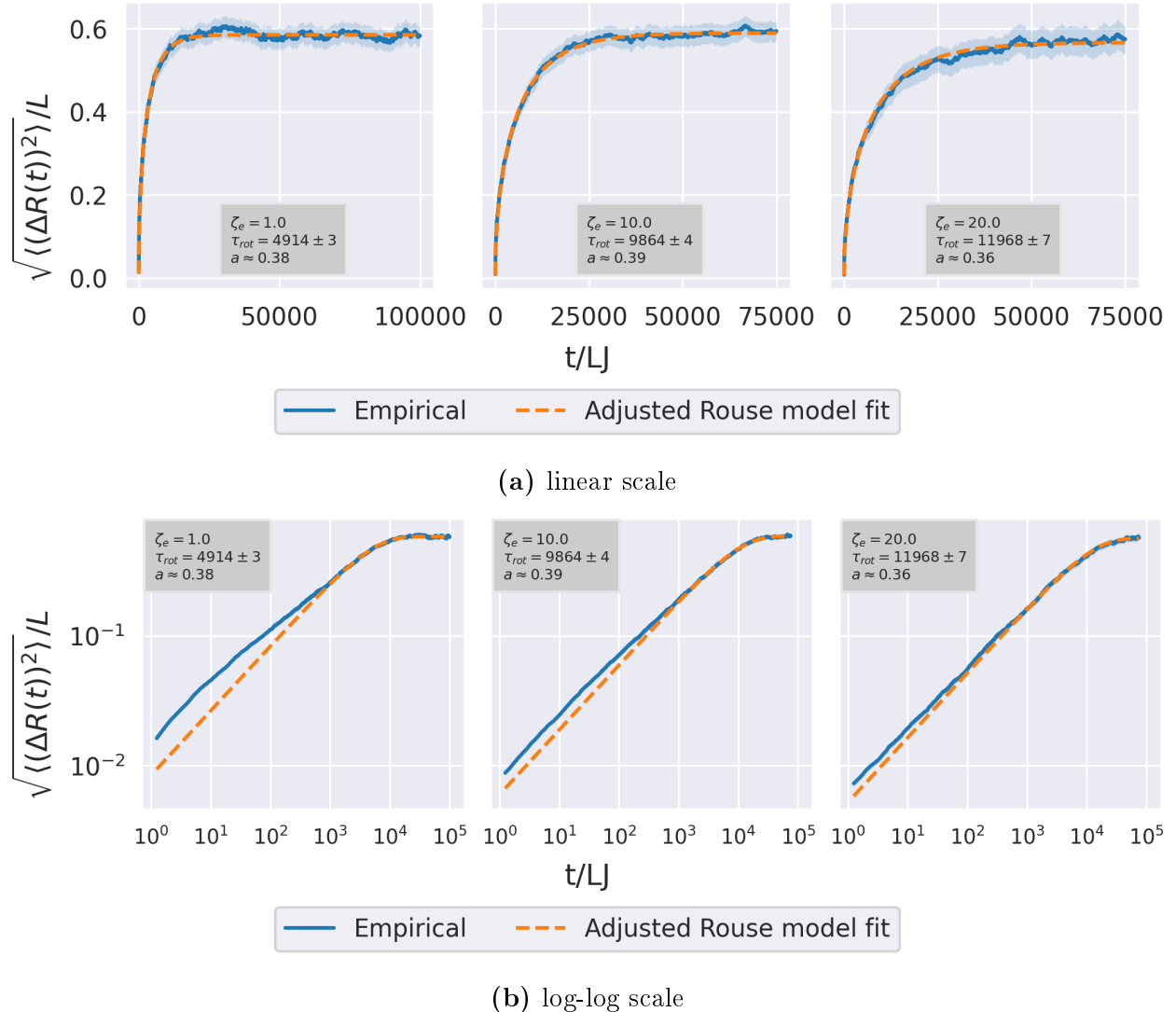


Figure 10: Empirical MSD of ETE of anchored chains with different values of the friction coefficient of the chain end ζ_e and a corresponding fit of the Adjusted Rouse model (Eq.50).

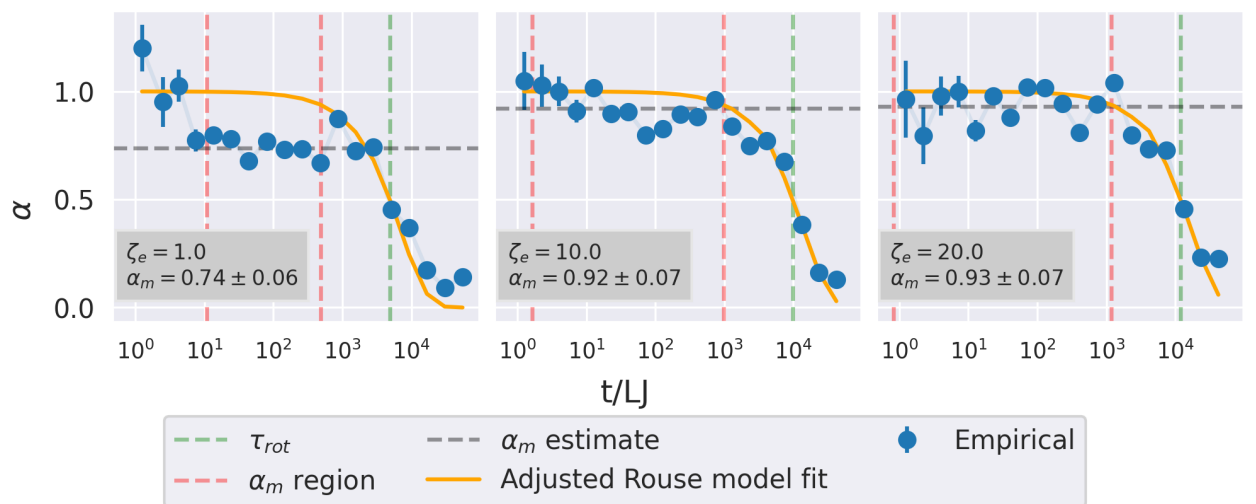


Figure 11: Scaling exponent α of MSD of ETE of anchored chains with different values of friction coefficient of the chain end ζ_e (blue dots). Scaling exponent α of corresponding fit (section 3.1.3, paragraph: Comparison with the Rouse model) of the adjusted Rouse model (Eq.50, orange line). Estimated scaling exponent for the time interval $t \ll \tau_{rot}$: α_m (grey dashed line); Red dashed lines correspond to α_m scaling region which is estimated as: $[10^{m_e/\zeta_e}, 10^{t_{rot}/10}]$

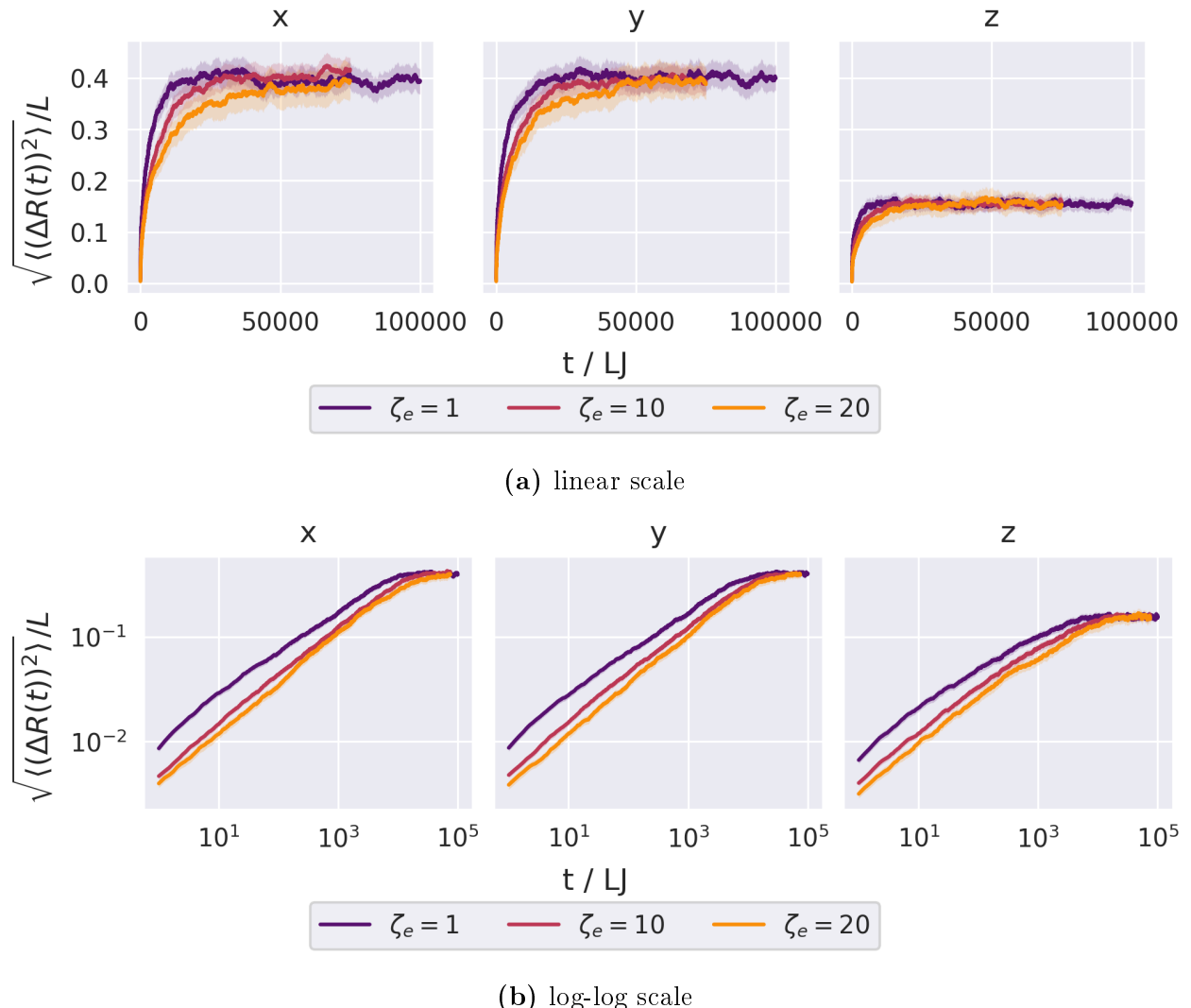


Figure 12: Empirical MSD of ETE of anchored chains with different values of the friction coefficient of the chain end ζ_e in main-axis system by dimension.

3.2. Free chain dynamics

The following section focuses on the study of the dynamics of the free polymer chains. Specifically the focus is on the verification of the hypothesis arising from the discussion in the paper of Singh *et. al.* [10]. Their work shows, that upon the binding of RAB5 to the EEA1 the scaling behavior of MSDLM shifts in the early time regime from 3/4 to the 2/3. This behavior is explained with the change of stiffness of the EEA1 upon the binding of RAB5, because the scaling regime of MSDLM $\alpha = 3/4$ corresponds the chains in the rod limit and the $\alpha = 2/3$ to the fully flexible chains in presence of hydrodynamic interactions. The persistence length is estimated indirectly by fitting the equation of MSDLM [10] derived by Hinczewski *et al.* [5]. Therefore this approach does not prove that a change of the scaling behavior is necessarily caused by the change of stiffness. An other factor possibly affecting the scaling behavior is the increased friction coefficient of the end of the chain caused by the bonded RAB5. Hence in this section the impact of the increased friction coefficient of the chain end (ζ_e) on the scaling behavior of MSDLM is explored. Additionally it is checked whether by changing the chain l_p from the estimated for EEA1 value ($l_p/L_{\text{EEA1}} \approx 3.01$ [10]) to the estimated for EEA1+RAB5 value ($l_p/L_{\text{EEA1+RAB5}} \approx 0.3$ [10]) causes a change of its scaling behavior similar to the experimentally observed change. Some simplifications are made to reduce the computational resources requirements and implementation complexity of simulation and analysis: the number of beads of the chain is set to $N_b = 64$ which results in a contour length $L = 61.11\text{LJ}$, which then corresponds to the contour length of EEA1, $L_{\text{EEA1}} \approx 222\text{nm}$.

When doing the analysis of the simulation data it is possible to calculate MSD of one or another chain end. In case of the symmetric chains, where $\zeta_e = \zeta = 1$, both ends should deliver same (within confidence interval) results. In case of asymmetric chains, where $\zeta_e > \zeta$, the results can be different. In this study both chain ends are analyzed. We refer to the chain end, for which ζ_e is set, as larger chain end and to the chain end, for which ζ is never changed, as smaller chain end. The smaller chain end corresponds to the chain end measured by Singh *et al.* [10].

For the larger chain end the obtained MSDLM curves are shown in Figure 13, the estimated scaling behavior in Figure 14 and the corresponding α_{min} values are available in Table 3. For the smaller chain end the obtained MSDLM curves are shown in Figure 17, the estimated scaling behavior in Figure 18 and the corresponding α_{min} values are available in Table 4. As a plausibility check the estimated scaling behavior of fully flexible free chains is displayed in Figure 15.

Larger chain end Firstly, $\alpha_{min} \approx 0.727$ in case $l_K/L = 6.02$, $\zeta_e = \zeta = 1$ approaches the expected value for the chain in the rod limit ($3/4$) and ≈ 0.5 (Figure 15) in case of the fully flexible chain matches almost exactly the expected value ($1/2$), which indicates a high reliability of the method.

Secondly, a drop of α_{min} is observed (from 0.727 ± 0.001 to 0.659 ± 0.002 , $\Delta \approx 0.068$) during the transition from $l_K/L = 6.02$ to the $l_K/L = 0.6$ by $\zeta_e = \zeta = 1$ (Figure 14).

Thirdly, it is observed, that an increase of ζ_e from $\zeta_e = \zeta = 1$ to $\zeta_e = 10$ causes a non-negligible increase of α_{min} : In case $l_K/L = 6.02$ from 0.727 ± 0.001 to 0.803 ± 0.001 , $\Delta \approx 0.076$. In case $l_K/L = 0.6$ from 0.659 ± 0.002 to 0.775 ± 0.001 , $\Delta \approx 0.116$. Given also the MSDLM curves in Figure 13, one can conclude, that the change in ζ_e affects the dynamics of the chains which is reflected in the behavior of the MSD of the larger chain end. Therefore when using the fit of analytical expression of MSDLM to the empirical MSD of the larger chain end to estimate some properties of the chain, one needs to account for the increased ζ_e to obtain more precise estimates.

ζ_e	l_K/L	τ_1	τ_b	τ_0	α_{min}	$\Delta\alpha_{min}$
1	6.02	78162.53	11.00	0.94	0.727	0.001
10	6.02	781625.32	1.65	9.41	0.803	0.001
1	0.6	6352.27	11.00	0.94	0.659	0.002
10	0.6	63522.69	1.65	9.41	0.775	0.001

Table 3: Free chains with different stiffness and end-bead friction values: Estimated values of the minimum of the scaling exponent α and characteristic time scales. The larger chain end is measured.

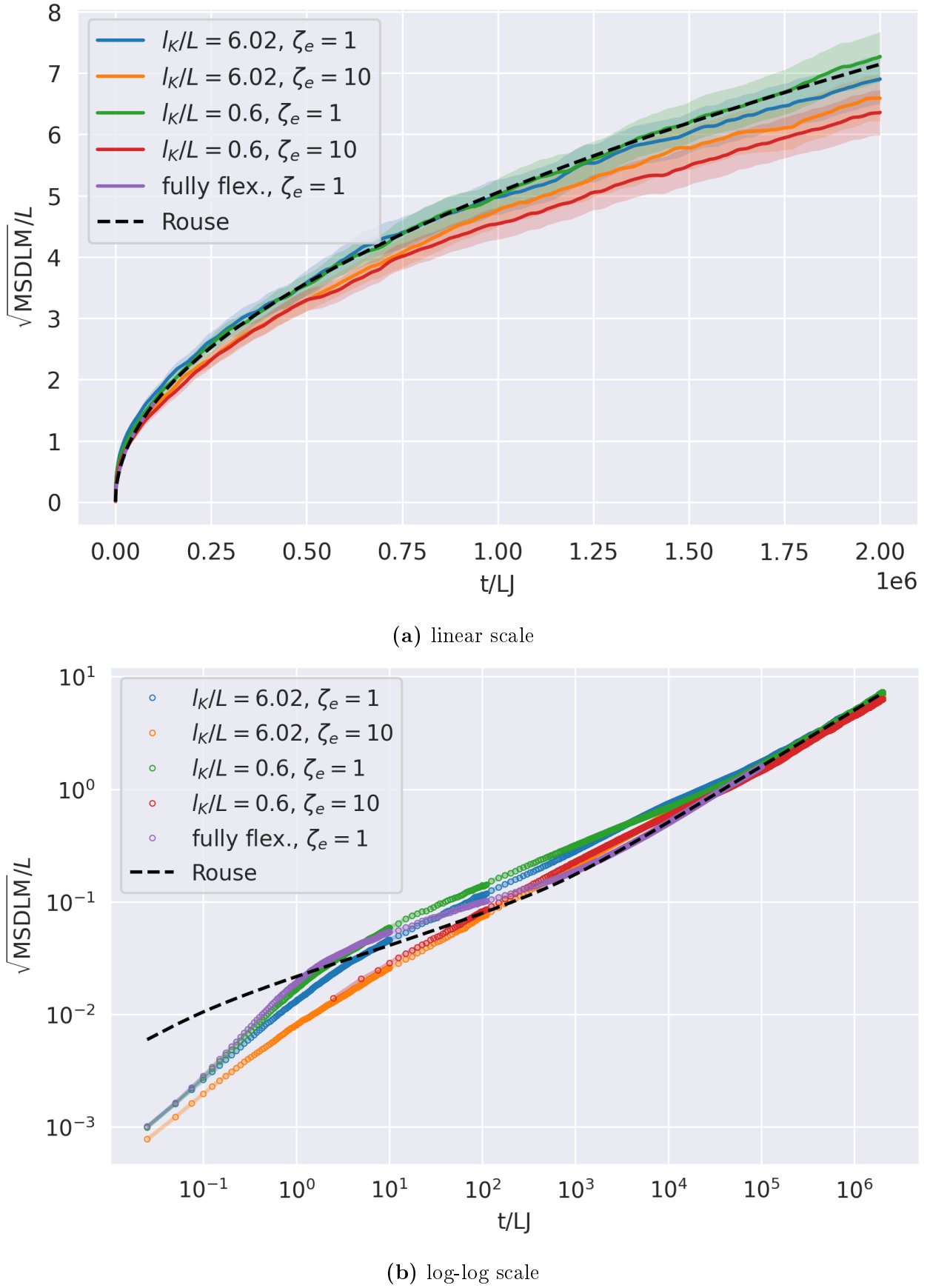


Figure 13: Empirical MSD of chain end (MSDLM) of free chains with different stiffness and end-bead friction values and Rouse model prediction for fully flexible chains. The larger end of the chain was measured.

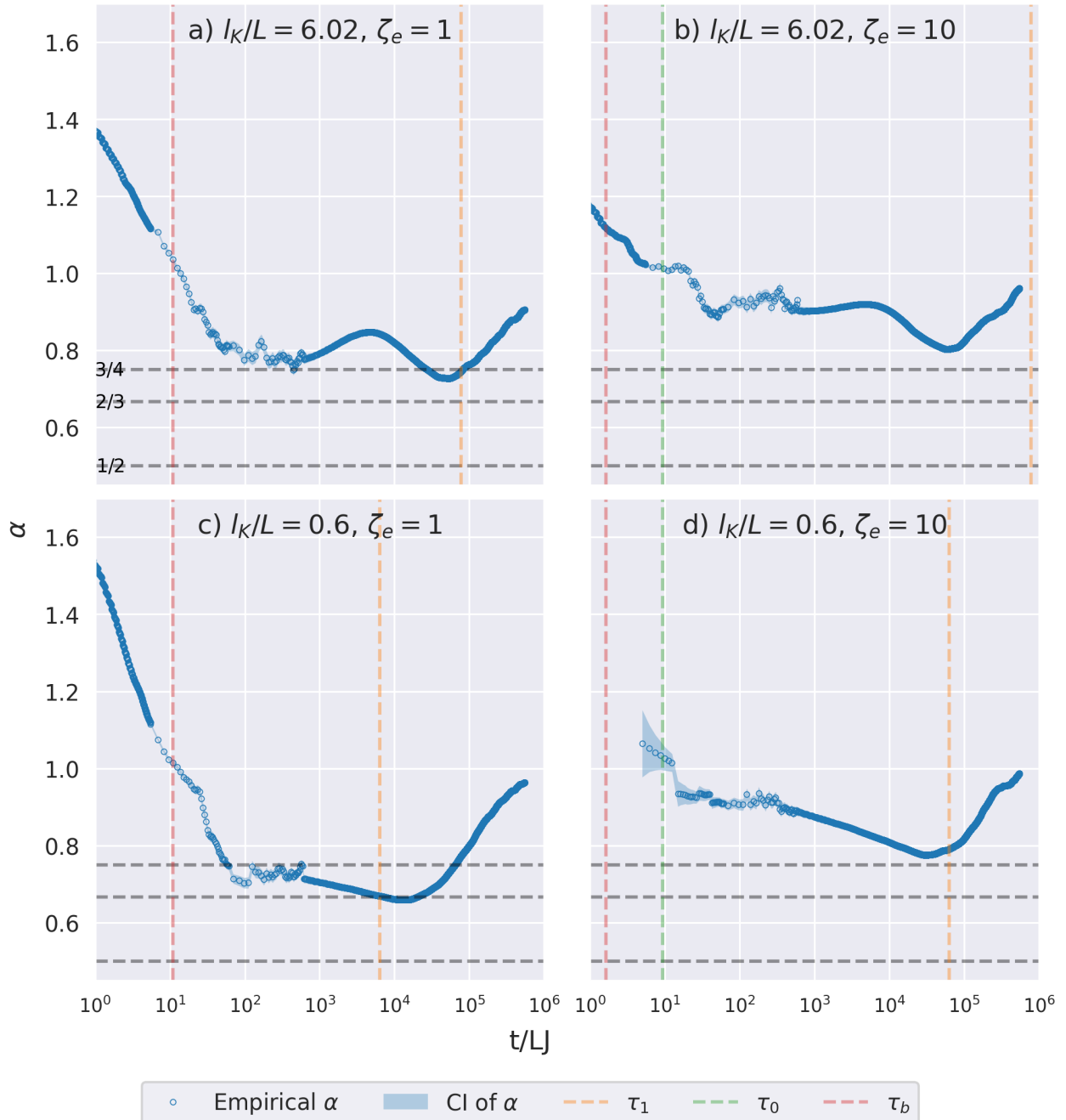


Figure 14: Scaling exponent α of MSD of chain end (MSDLM) of free chains with different stiffness and end-bead friction values; Grey dashed lines correspond to $3/4, 2/3, 1/2$ values. The larger end of the chain was measured.

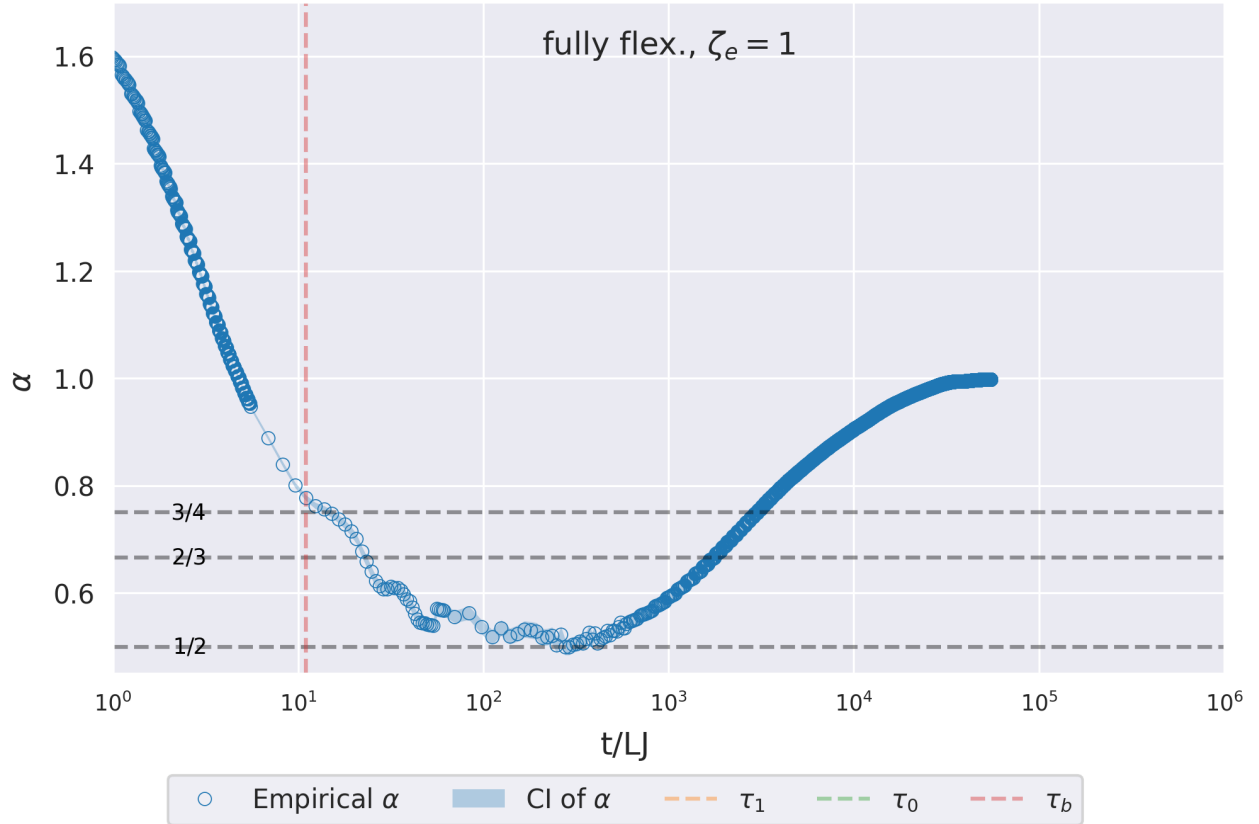


Figure 15: Scaling exponent α of MSD of chain end (MSDLM) of free full flexible chain. τ_0 and τ_b are outside of the x-axis boundaries. Estimated $\alpha_{min} = 0.499 \pm 0.015$.

Smaller chain end Firstly, we note, that the $\alpha_{min} = 0.73 \pm 0.02$ in case $l_K/L = 6.02$, $\zeta_e = \zeta = 1$ approaches the expected value for the chain in the rod limit ($3/4$) and the $\alpha_{min} = 0.652 \pm 0.002$ in case $l_K/L = 0.6$, $\zeta_e = \zeta = 1$ is between $1/2$ and $3/4$ in agreement with the theoretical expectations. This is, similarly to the case of the larger chain end, an indication for the high reliability of the method.

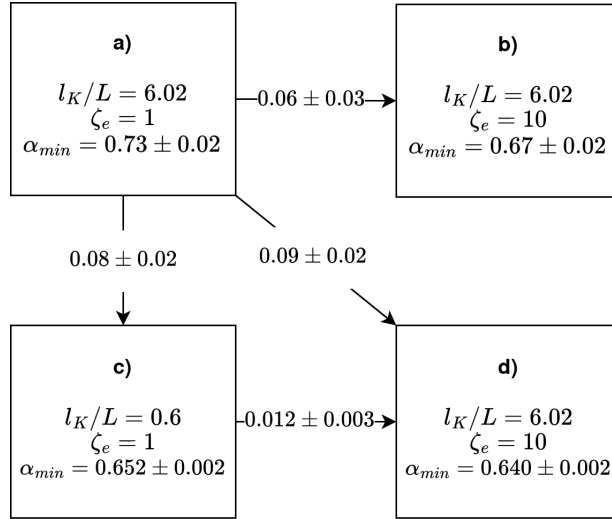


Figure 16: Overview of cases in simulations of free chains. Arrows represent discussed transitions. A change of α_{min} ($\Delta\alpha_{min}$, as defined in Eq. 51, Eq. 52, Eq. 53) is written on the arrow.

Secondly, a drop of α_{min} is observed during the transition from $l_K/L = 6.02$ to the $l_K/L = 0.6$ by $\zeta_e = \zeta = 1$ (Figure 18, $a \rightarrow c$, Figure 19):

$$\begin{aligned}\alpha_{min}(a) &:= \alpha_{min}(l_K/L = 6.02, \zeta_e = 1) = 0.73 \pm 0.02 \\ \alpha_{min}(c) &:= \alpha_{min}(l_K/L = 0.6, \zeta_e = 1) = 0.652 \pm 0.002 \\ \Delta\alpha_{min}(a \rightarrow c) &:= \Delta\alpha_{min}(l_K/L = 6.02, \zeta_e = 1 \rightarrow l_K/L = 0.6, \zeta_e = 1) = 0.08 \pm 0.02\end{aligned}\quad (51)$$

Both values are very close (however the second one is outside the CI, which can be explained with absence of hydrodynamic and excluded volume interactions) to the ones of Singh *et al.* [10]. Moreover, $\Delta\alpha_{min}(a \rightarrow c)$ is in agreement with the change of α_{min} from EEA1 to EEA1+RAB5 (≈ 0.083) obtained by Singh *et al.* [10]. However, in case $l_K/L = 0.6$ α_{min} is far larger than α_{min} of the fully flexible chain in contrast with the results of Singh *et al.* [10] ($\alpha_{min} \approx 3/4$ for EEA1 and $\alpha_{min} \approx 2/3$ for EEA1+RAB5) where $\alpha_{min} = 2/3$ matches the one of the fully flexible chain, taking into account the presence of excluded volume interactions.

Thirdly, it is observed, that an increase of ζ_e from $\zeta_e = \zeta = 1$ to $\zeta_e = 10$ (Figure 18, $a \rightarrow b$, $c \rightarrow d$) causes, in contrast to the larger chain end, a non-negligible decrease of the α_{min} (Figure 19):

$$\begin{aligned}\alpha_{min}(b) &:= \alpha_{min}(l_K/L = 6.02, \zeta_e = 10) = 0.67 \pm 0.02 \\ \alpha_{min}(d) &:= \alpha_{min}(l_K/L = 0.6, \zeta_e = 10) = 0.640 \pm 0.002 \\ \Delta\alpha_{min}(a \rightarrow b) &:= \Delta\alpha_{min}(l_K/L = 6.02, \zeta_e = 1 \rightarrow l_K/L = 6.02, \zeta_e = 10) = 0.06 \pm 0.03 \\ \Delta\alpha_{min}(c \rightarrow d) &:= \Delta\alpha_{min}(l_K/L = 0.6, \zeta_e = 1 \rightarrow l_K/L = 0.6, \zeta_e = 10) = 0.012 \pm 0.003\end{aligned}\quad (52)$$

One can conclude, that a change of the friction coefficient of the chain end affects the scaling behavior of the MSD of the smaller chain end, decreasing corresponding scaling exponent α in the region of the subdiffusive motion. However, the influence decreases with decreasing stiffness of the chain. The change $\Delta\alpha_{min}(a \rightarrow b)$ is also in agreement (within the CI) with the change of α_{min} by RAB5 binding to the EEA1 (≈ 0.083) obtained by Singh *et al.* [10].

Furthermore, analyzing the transition $a \rightarrow d$ (Figure 18, $a \rightarrow d$), which models the transition from EEA1 to the EEA1+RAB5, one can see the decrease of α_{min} (Figure 19):

$$\Delta\alpha_{min}(a \rightarrow d) := \Delta\alpha_{min}(l_K/L = 6.02, \zeta_e = 1 \rightarrow l_K/L = 0.6, \zeta_e = 10) = 0.09 \pm 0.02 \quad (53)$$

Apart from $\alpha_{min}(d)$ being close, but outside the CI (which can be explained with the absence of hydrodynamic and excluded volume interactions), to the α_{min} of EEA1+RAB5, this result is qualitatively and quantitatively compatible with the change of α_{min} observed by Singl *et al.* [10] (from 3/4 to the 2/3, $\Delta \approx 0.083$).

To summarize, we have shown, that both, stiffness transition of the chain and a 10x increase of the friction coefficient of the chain end can cause a decrease in the minimum of the scaling exponent α .

ζ_e	l_K/L	τ_1	τ_b	τ_0	α_{min}	$\Delta\alpha_{min}$
1	6.02	78162.53	1.65	0.94	0.73	0.02
10	6.02	78162.53	1.65	0.94	0.67	0.02
1	0.6	6352.27	1.65	0.94	0.652	0.002
10	0.6	6352.27	1.65	0.94	0.640	0.002

Table 4: Free chains with different stiffness and end-bead friction values: Estimated values of the minimum of the scaling exponent α and characteristic time scales. The smaller chain end is measured.

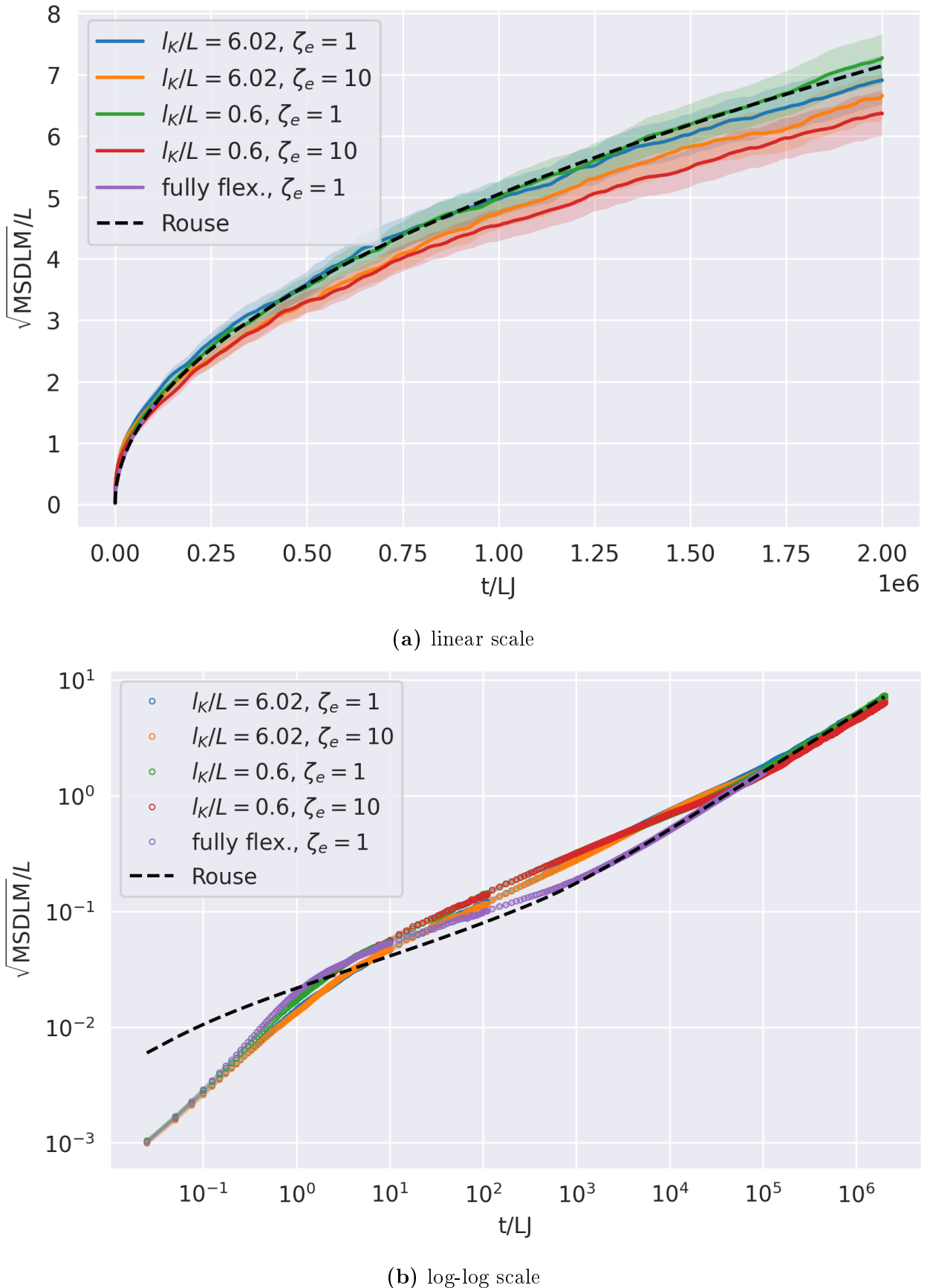


Figure 17: Empirical MSD of chain end (MSDLM) of free chains with different stiffness and end-bead friction values and Rouse model prediction for fully flexible chains. The smaller end of the chain was measured.

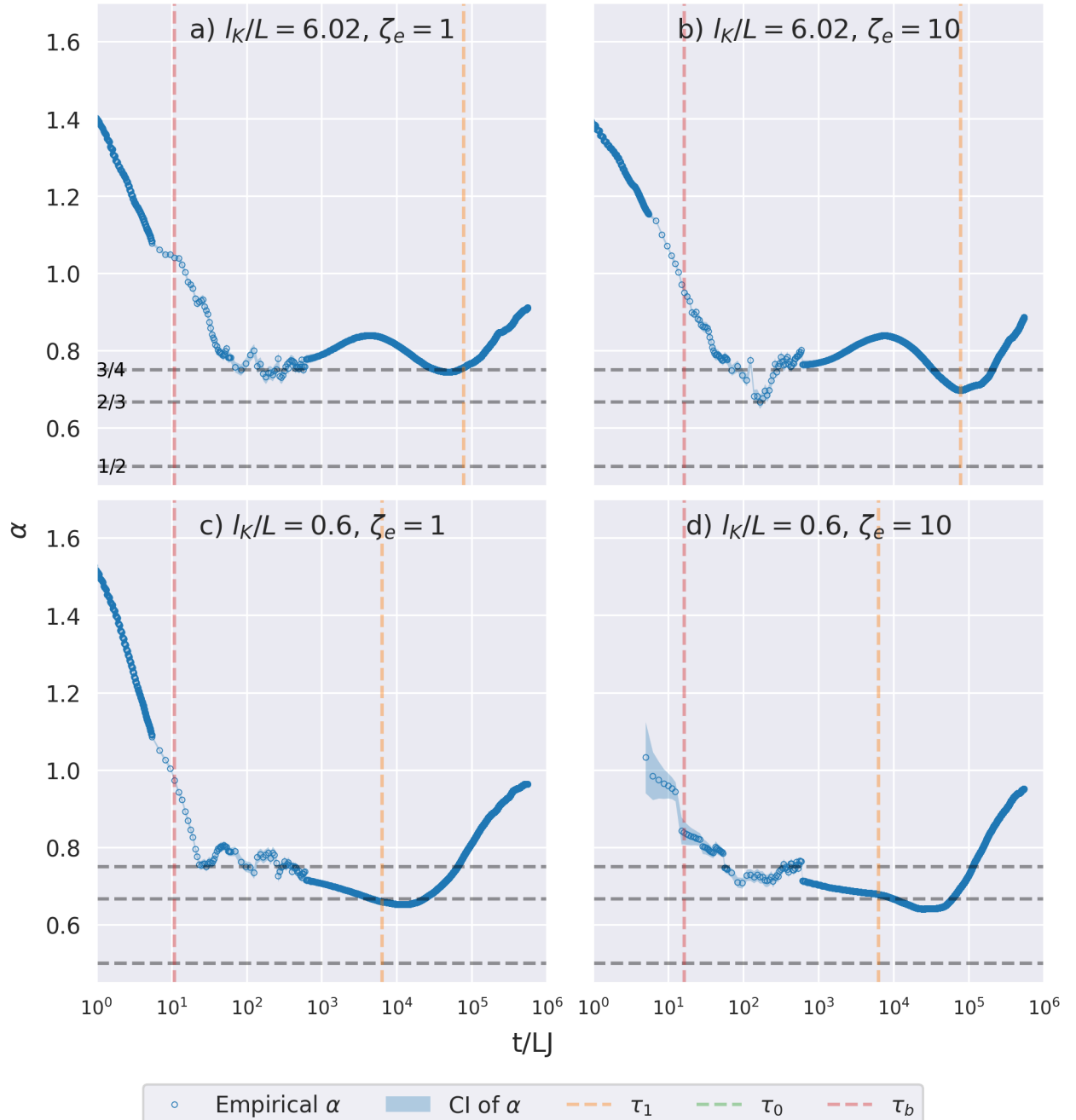


Figure 18: Scaling exponent α of MSD of chain end (MSDLM) of free chains with different stiffness and end-bead friction values; Grey dashed lines correspond to $3/4$, $2/3$, $1/2$ values. The smaller end of the chain was measured.

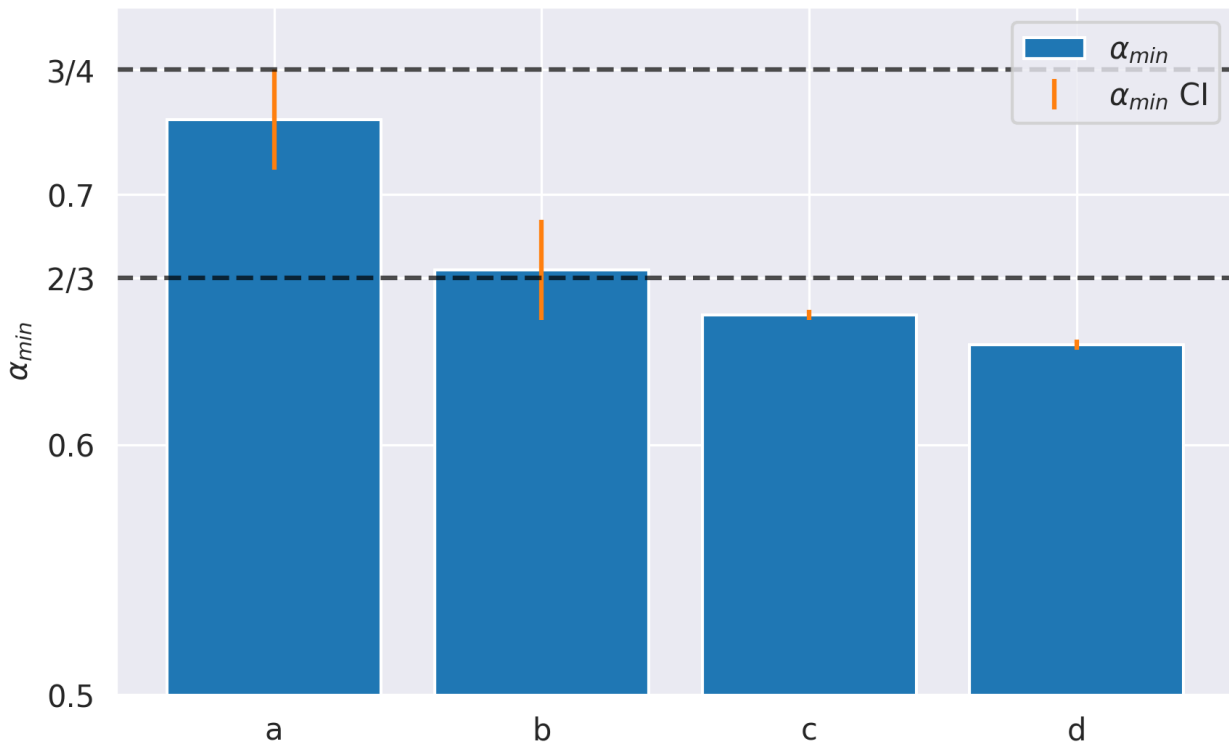
(a) α_{min} , smaller end of the chain(b) $\Delta\alpha_{min}$, smaller end of the chain

Figure 19: α_{min} and $\Delta\alpha_{min}$ of the MSD of the smaller end of the free chain. Notation follows Figure 18, Eq. 51, Eq. 52, Eq. 53.

4. Summary and Outlook

Multiple simulations are performed varying the chain stiffness and friction coefficient of the chain end, ignoring the hydrodynamic and excluded volume interactions. The resulting trajectories are processed and carefully analyzed.

Anchored chains The specific dynamical quantity, mean squared displacement of end-to-end distance (MSD of ETE, in following: MSD), was considered.

It is shown, that the relaxation of the free fully flexible chain is faster then the relaxation of the anchored one ($\tau_{R,\text{free}} < \tau_{R,\text{anchored}}$). As expected, the predictions of the Rouse model with free boundary conditions for the fully flexible chains do not hold for anchored fully flexible chains. However, it is observed, that the predictions of the Rouse model with free boundary conditions for the fully flexible chains with τ_R as free parameter hold for anchored fully flexible chains (Figure 2). The estimation of τ_R for anchored fully flexible chains delivers the correction factor required to account for anchoring.

In case of the semiflexible chain several conclusions can be made. As expected, Rouse model predictions for flexible chains quickly deviate from observations made for semiflexible chains even with small stiffness ($l_p/L \approx 0.15$). It is shown, that the MSD of anchored semiflexible chains, similar to the case of full flexible chains, obeys the same proportionality ($\propto \exp\left(-\frac{t}{\tau_{rot}}\right)$) as anchored semiflexible chains for longer time scales, however with different values of characteristic time τ_{rot} . These characteristic times τ_{rot} are estimated for different values of stiffness. It was observed, that τ_{rot} grows with increasing stiffness of the chain. To explore the shorter time scales, the transient scaling exponent α of the MSD (defined in Section 2.2.3, Eq. 47) is computed. In the region of subdiffusive motion with $t \ll \tau_{rot}$ the values of the scaling exponent α match qualitatively the expected minimum values of the scaling exponent of free chains. Furthermore, the MSD was considered in a decomposition in the "main-axis" coordinate system (Section 2.2.2). It is shown, that the difference of MSD dimension parallel to the main axis with MSD dimensions perpendicular to the main axis increases with growing l_p , specifically, the parallel dimension is characterized through smaller relaxation time and a lower value in the long time limit.

Further the impact of the friction coefficient of the chain end (ζ_e) on the dynamical properties of semiflexible chain in the rod limit was studied. The specific value of $l_p/L = 3.01$ was selected to match the stiffness of EEA1. Similarly to the study of impact of chain stiffness, it is shown, that a proportionality ($\propto \exp\left(-\frac{t}{\tau_{rot}}\right)$) holds for $t > \tau_{rot}$ if τ_{rot} is considered as a free parameter. The increase of the estimated τ_{rot} with rising ζ_e is observed. $\alpha(t)$ was calculated and the α value in the region of subdiffusive motion (here called α_m) was estimated. A small

increase of α_m ($0.74 \pm 0.06 \rightarrow 0.92 \pm 0.07$) by the increase of ζ_e from 1 to 10 was observed and no difference was observed during an increase of ζ_e from 10 to 20. Additionally, different projections of the MSD were considered in the "main-axis" coordinate system, however, the effects of increased ζ_e are visually shown to be consistent across the different dimensions.

Free chains The specific dynamical quantity, MSD of the chain end (in following: MSDLM), was evaluated for both the larger chain end and the smaller chain end (following the naming convention introduced in Section 3.2). The scaling exponent $\alpha(t)$ of MSDLM was examined.

For the larger chain end we conclude: α_{min} significantly decreases by the change from $l_p/L = 3.01$ to $l_p/L = 0.3$ in case of $\zeta = \zeta_e = 1$. Both values are in agreement with theoretical expectations. Furthermore it is shown, that by increasing ζ_e , the minimum of the scaling exponent α_{min} is also significantly increased in both cases: rod like $l_p/L \approx 3.01$ (matches the estimate for EEA1 in [10]) and coil like $l_p/L \approx 0.3$ (matches the estimate for EEA1+Rab5 in [10]). Therefore, taking into account the observed MSDLM curves, the conclusion is made, that when using the fit of analytical expression of MSDLM to the empirical MSD of larger chain end to estimate some properties of the chain, one needs to account for an increased ζ_e to obtain more precise estimates.

For the smaller chain end we conclude: α_{min} significantly decreases by the stiffness decrease $a \rightarrow c$ (Eq. 51, Figure 18: a, c , Figure 19). Both values are in agreement with theoretical expectations. $\alpha_{min}(a)$ matches within the confidence interval α_{min} of EEA1 obtained by Singh *et al.* [10]. $\alpha_{min}(c)$ does not match α_{min} of EEA1+RAB5 obtained by Singh *et al.* [10], which can be explained with an absence of excluded volume and hydrodynamic interactions in the simulation. However, the difference, $\Delta\alpha_{min}(a \rightarrow c)$, matches within the confidence interval the one observed by Singh *et al.* [10]. Furthermore, it is shown, that increase of the ζ_e ($a \rightarrow b$, $c \rightarrow d$) causes a decrease of α_{min} (Eq. 52, Figure 18, Figure 19), although this decrease is less pronounced than in the case of a reduction of the chain stiffness. The difference, $\Delta\alpha_{min}(a \rightarrow b)$ matches, within the CI, the one observed by Singh *et al.* [10]. $\alpha_{min}(d)$ is close, however outside of the CI, to the one observed by Singh *et al.* [10], which is explained with absence of hydrodynamic and excluded volume interactions in the simulation. The difference, $\Delta\alpha_{min}(a \rightarrow d)$, is in agreement, within the CI, to the one observed by Singh *et al.* [10]. Therefore, we have shown, that both, stiffness transition of the chain and 10x increase of friction coefficient of the chain end can cause the change of α_{min} , as observed by Singh *et al.* [10] upon the binding of RAB5 to the EEA1. However, if, following the binding of RAB5 to EEA1, the friction coefficient at the EEA1 chain end increases by a factor of less than 10, then our simulations have overemphasized the effects of the larger chain end. Under this circumstance, it is worth noting, that $\Delta\alpha_{min}(a \rightarrow b)$ is much less likely to match the one experimentally observed by

Singh *et al.* [10], than $\Delta\alpha_{min}(a \rightarrow c)$ (see Figure 19). Therefore, we hypothesize, that an increase of ζ_e , reasonably smaller then 10, would not explain the change of α_{min} observed by Singh *et al.* [10].

Outlook There are several limitations of this work, which can be improved in the future research. Firstly it is necessary to increase the chain contour length L to better match both the theoretical requirement $l_b \ll L$ and the length of the EEA1 chain. Also, one needs to consider the smaller value of ζ_e to verify our hypothesis. Then, an improvement would be to consider a grid of l_p and ζ_e values to obtain the curves of characteristic times and α_{min} values in dependence of l_p and ζ_e . Of specific interest is the value of ζ_e which matches the value of real Rab5 bound to the end of EEA1. Finally, one needs to consider hydrodynamic and excluded volume interactions, which may have significant impact on the dynamical properties.

Appendices

A. Code

Code is available at: <https://github.com/RikiTikkiTavi/polyflexmd>

5. References

- [1] M. Doi. *Introduction to Polymer Physics*. Oxford University Press, 1997.
- [2] M. Doi and S. F. Edwards. *The Theory of Polymer Dynamics*. Oxford University Press, 1994.
- [3] B. DÜNWEG and W. PAUL. Brownian dynamics simulations without gaussian random numbers. *International Journal of Modern Physics C*, 02(03):817–827, 1991.
- [4] C. R. Harris, K. J. Millman, S. J. van der Walt, R. Gommers, P. Virtanen, D. Cournapeau, E. Wieser, J. Taylor, S. Berg, N. J. Smith, R. Kern, M. Picus, S. Hoyer, M. H. van Kerkwijk, M. Brett, A. Haldane, J. F. del Río, M. Wiebe, P. Peterson, P. Gérard-Marchant, K. Sheppard, T. Reddy, W. Weckesser, H. Abbasi, C. Gohlke, and T. E. Oliphant. Array programming with NumPy. *Nature*, 585(7825):357–362, Sept. 2020.
- [5] M. Hinczewski and R. R. Netz. Global cross-over dynamics of single semiflexible polymers. *Europhysics Letters*, 88(1):18001, oct 2009.
- [6] K. Kremer and G. S. Grest. Dynamics of entangled linear polymer melts: A molecular-dynamics simulation. *The Journal of Chemical Physics*, 92(8):5057–5086, 04 1990.
- [7] R. H. C. Michael Rubingstein. *Polymer Physics*. Oxford University Press, 2005.
- [8] D. H. Murray, M. Jahnel, J. Lauer, M. J. Avellaneda, N. Brouilly, A. Cezanne, H. Morales-Navarrete, E. D. Perini, C. Ferguson, A. N. Lupas, Y. Kalaidzidis, R. G. Parton, S. W. Grill, and M. Zerial. An endosomal tether undergoes an entropic collapse to bring vesicles together. *Nature*, 537(7618):107–111, Aug. 2016.
- [9] A. Nikoubashman, A. Milchev, and K. Binder. Dynamics of single semiflexible polymers in dilute solution. *The Journal of Chemical Physics*, 145(23):234903, 12 2016.
- [10] A. Singh, J. A. Soler, J. Lauer, S. W. Grill, M. Jahnel, M. Zerial, and S. Thutupalli. Gtpase-dependent cyclic flexibility transitions drive the two-component eea1-rab5 molecular motor. *bioRxiv*, 2022.
- [11] C. Svaneborg and R. Everaers. Characteristic time and length scales in melts of kremer-grest bead-spring polymers with wormlike bending stiffness. *Macromolecules*, 53(6):1917–1941, 2020.
- [12] W. C. Swope, H. C. Andersen, P. H. Berens, and K. R. Wilson. A computer simulation method for the calculation of equilibrium constants for the formation of physical clusters of molecules: Application to small water clusters. *The Journal of Chemical Physics*, 76(1):637–649, 01 1982.

- [13] A. P. Thompson, H. M. Aktulga, R. Berger, D. S. Bolintineanu, W. M. Brown, P. S. Crozier, P. J. in 't Veld, A. Kohlmeyer, S. G. Moore, T. D. Nguyen, R. Shan, M. J. Stevens, J. Tranchida, C. Trott, and S. J. Plimpton. LAMMPS - a flexible simulation tool for particle-based materials modeling at the atomic, meso, and continuum scales. *Comp. Phys. Comm.*, 271:108171, 2022.
- [14] P. Virtanen, R. Gommers, T. E. Oliphant, M. Haberland, T. Reddy, D. Cournapeau, E. Burovski, P. Peterson, W. Weckesser, J. Bright, S. J. van der Walt, M. Brett, J. Wilson, K. J. Millman, N. Mayorov, A. R. J. Nelson, E. Jones, R. Kern, E. Larson, C. J. Carey, İ. Polat, Y. Feng, E. W. Moore, J. VanderPlas, D. Laxalde, J. Perktold, R. Cimrman, I. Henriksen, E. A. Quintero, C. R. Harris, A. M. Archibald, A. H. Ribeiro, F. Pedregosa, P. van Mulbregt, and SciPy 1.0 Contributors. SciPy 1.0: Fundamental Algorithms for Scientific Computing in Python. *Nature Methods*, 17:261–272, 2020.

Acknowledgement

First of all I would like to express my gratitude to Prof. Dr. Jens-Uwe Sommer, for providing me with the opportunity to write my bachelor thesis at the Institute Theory of Polymers, for all constructive feedback, for the initial assessment of my work and professional advice.

I would also like to extend my gratitude to the second assessor of my thesis, Prof. Dr. Arash Nikoubashman.

I am sincerely grateful to my supervisor, Dr. Holger Merlitz, for the invaluable guidance and support throughout this academic journey. Specifically, I deeply appreciate his mentorship in understanding the theoretical framework, his guidance in navigating LAMMPS, his professional advice and his proofreading of my thesis.

A special and warm thanks to my loving wonderful wife, Zlata, for her support during all my studies, always being there for me, being my light during the dark times. I would like to thank my family, especially my parents (Aliaksandr and Valiantsina), grandparents (Anna, Leonid, Liudmila), sister (Maria) and parents-in-law (Vladimir and Tatjana). And, of course, a big thanks to my cat, Proton, for contributing to my mental well-being.

Erklärung

Hiermit erkläre ich, dass ich diese Arbeit im Rahmen der Betreuung am Leibniz-Institut für Polymerforschung Dresden e. V. ohne unzulässige Hilfe Dritter verfasst und alle Quellen als solche gekennzeichnet habe.

Yahor Paromau

Dresden, November 2023